

To the Graduate Council:

I am submitting herewith a thesis written by Charles A. Burchfield entitled "Column Capacity Analysis For Determining Blast Resistance Of Steel Structures In Multi-Hazard Design And Evaluation." I have examined the final copy of this thesis for form and content and recommend that it be accepted in partial fulfillment of the requirements for the degree of Master of Science, with a major in Civil Engineering.

---

Christopher Mullen, Major Professor  
Associate Professor

We have read this thesis  
and recommend its acceptance:

---

Ahmed Al-Ostaz, Associate Professor

---

Elizabeth Ervin, Assistant Professor

Accepted for the Council:

---

Dean of the Graduate School

## STATEMENT OF PERMISSION TO USE

In presenting this thesis in partial fulfillment of the requirements for a Master's degree at The University of Mississippi, I agree that the Library shall make it available to borrowers under rules of the Library. Brief quotations from this thesis are allowable without special permission, provided that accurate acknowledgment of the source is made.

Permission for extensive quotation from or reproduction of this thesis may be granted by my major professor or in his absence, by the Head of Interlibrary Services when, in the opinion of either, the proposed use of the material is for scholarly purposes. Any copying or use of the material in this thesis for financial gain shall not be allowed without my written permission.

Signature\_\_\_\_\_

Date\_\_\_\_\_

COLUMN CAPACITY ANALYSIS FOR DETERMINING BLAST RESISTANCE OF  
STEEL STRUCTURES IN MULTI-HAZARD DESIGN AND EVALUATION

A Thesis

Presented for the

Master of Science

Degree

The University of Mississippi

Charles A. Burchfield

December 2009

## DEDICATION

This work is dedicated to my parents, Randy and Sharon Burchfield, for their unwavering support and motivation.

## ACKNOWLEDGMENTS

I would like to thank, first and foremost, my parents, Randy and Sharon Burchfield. Without them, I would not have made it through to completion. Their encouragement has been a source of strength and motivation.

There are numerous acknowledgments from The University of Mississippi. Thank you to all of my professors through the years from undergraduate to graduate. Thank you to the staff in the Civil Engineering Department, Mrs. Dorothy Lloyd and Gene Walker, without their assistance none of this work could have been accomplished. A special thanks to Dr. Ahmed Al-Ostaz and Dr. Elizabeth Ervin for providing me guidance and suggestions throughout this work. Thank you to Dr. Christopher Mullen for his guidance over the past few years.

Special thanks goes out to my classmates over the past few years, especially Hunain Alkhateb, Jessica Headrick, Mohammad Irshidat, Tyler Kidd, and Katherine Osborne, without their help and assistance the class load would have been overwhelming. Nothing would have been possible without Tezeswi Tadepalli, whose work proceeded, provided motivation, and insight into my work. The contributions from Tez are priceless and greatly appreciated.

This research was funded by the Department of Homeland Security-sponsored Southeast Region Research Initiative (SERRI) at the Department of Energy's Oak Ridge National Laboratory.

## ABSTRACT

In recent years, much has been done in the field of blast analysis and design. Numerous papers and articles have been written on varying topics from proper application of blast loads to structural response. A major main point to glean from each paper is that the best way to mitigate blast damage or exposure is to increase the stand-off distance at which a charge can be placed. In most cases however, existing buildings do not have the capabilities to retrofit the buildings for further stand-off distances. Thus, it is critical to explore the response of structures to this extreme load case.

During a blast event, columns are often the most directly affected elements in a structure. Thus, an investigation into the response of columns is needed. In this study, W8x31 members were chosen from a design of a 3-story frame with 12 foot story heights using the International Building Code 2006 as discussed in the following chapter. Only a single column was chosen in the design for the largest loading case, interior lower level. The column was then used for all columns in the frame. This may contribute to a possible over-design; however, the assumption was made that this could be a realistic scenario for ease of construction. The column models were developed using Computers and Structures, INC.'s SAP2000 software. This software was chosen for its ability to perform nonlinear fiber modeling. Versions 12 and 14 were utilized. These results were then incorporated into the analysis of the three-dimensional frame.

With the column results, we can access the response of the three dimensional frame subjected to a large lateral load, specifically blast. The usage of the damage states pointed out in the column analysis allows the evaluation of column damage levels

throughout the structure. This grants the ability to access in greater detail the reliability of the damage structure in order to determine the resistivity of this particular frame to blast loading.

The assessment of the results of the columns and three-dimensional frame show interesting results. First, the results from the column analysis show the linear elastic, elastic buckling, and plastic responses. SAP2000 allows for the ability to take the column through its entire useful life. Using these results to determine the damage states, the three-dimensional frame is subjected to nine blast scenarios. Upon examination, the blast cases chosen for testing appear to be minor compared to the response. Most cases showed slight damage, but only one case showed major damage with the development of plastic hinges and displacements reaching collapse. It is also seen that increasing the standoff distance for a blast scenario is the most effective way to mitigate damage.

## TABLE OF CONTENTS

CHAPTER	PAGE
I. INTRODUCTION.....	1
1.1 Background.....	1
1.1.1 Beam to Column Connection.....	1
1.1.2 Beam-Column Analysis.....	3
1.1.3 Frame System Analysis.....	4
1.2 Motivation.....	6
II. COLUMN CAPACITY ANALYSIS.....	7
2.1 Background.....	7
2.2 Column Models.....	7
2.3 Analysis.....	9
2.3.1 Load Development.....	9
2.3.2 Model Cases.....	9
2.4 Analytical Calculations.....	10
2.4.1 Elastic Response.....	10
2.4.2 Elastic Buckling.....	12
2.4.3 Plastic Analysis.....	14
2.5 Computer Model Analysis.....	17
III. MULTI-HAZARD STEEL FRAME ANALYSIS.....	21
3.1 Background.....	21
3.2 Design.....	21

3.2.1 Slab Design.....	23
3.2.2 Composite Beam Design.....	23
3.2.3 Column Design.....	24
3.2.4 Seismic Design.....	26
3.2.5 Blast Loading.....	32
3.3 Frame Response to Blast Pressure.....	39
3.3.1 Close Standoff Distance.....	40
3.3.1.1 Low Yield Charge Weight.....	40
3.3.1.2 Medium Yield Charge Weight.....	41
3.3.1.3 High Yield Charge Weight.....	42
3.3.2 Medium Standoff Distance.....	43
3.3.2.1 Low Yield Charge Weight.....	44
3.3.2.2 Medium Yield Charge Weight.....	45
3.3.2.3 High Yield Charge Weight.....	45
3.3.3 Far Standoff Distance.....	46
IV. CONCLUSIONS AND RECOMMENDATIONS.....	48
4.1 Conclusions.....	48
4.2 Recommendations for Future Work.....	50
LIST OF REFERENCES.....	51
LIST OF APPENDICIES.....	54
Appendix A.....	55
Appendix B.....	56
VITA.....	57

## LIST OF FIGURES

FIGURE	PAGE
1-1. Traditional and "Side Plate®" Moment Connection Systems.....	2
1-2. DYNA3D Results for 60% Axial Load Subjected to Blast.....	4
1-3. Drift Ratios for Each Major Blast Case Studied.....	6
2-1. Default vs. User-Defined Fiber Locations.....	8
2-2. Column Models Used (Sketch) was Pin-Roller, Fixed-Free Rotation, and Fixed-Fixed Rotation.....	10
2-4. Column Model Sketch for Buckling Response Verification.....	12
2-5. Plastic in the Flange and Web and Plastic in the Flange Only .....	15
2-6. Location of Fiber Hinges for Fixed-Fixed and Other Two Cases .....	17
2-7. Moment-Rotation Curve for Fixed-Fixed Rotation.....	19
2-8. Force-Displacement Curve for Fixed-Fixed Rotation.....	19
3-1. 3-D Frame Sketch.....	22
3-2. Composite Slab Sketch.....	22
3-3. W8x31 Dimensions .....	25
3-4. Design Response Spectrum from ASCE/SEI 7-05 Figure 11.4-1 .....	28
3-5. Distribution of Total Base Shear .....	30
3-6. Base Shear Distributed Throughout the 3D Frame .....	30
3-7. Equivalent 2-D Frame for Dynamic Analysis .....	31
3-8. Time History Function for Earthquake Analysis.....	32
3-9. Hemispherical Blast Wave Diagram (Figure 2-14 TM5-1300).....	33

3-10. FEMA 426 Pressure-Time History.....	35
3-11. Hemispherical Blast Wave Parameters (Figure 2-15 TM5-1300).....	36
3-12. Possible Blast Charge Weights and Standoff (Figure 4-5 FEMA 436).....	37
3-13. Time History Function for Blast Analysis.....	38
3-14. Column Numbering System to Monitor Blast Effects.....	39
3-15. Joint Numbering System to Monitor Blast Effects.....	40

## LIST OF TABLES

TABLE	PAGE
2-1. Results from Elastic Calculations from AISC Manual.....	11
2-2. Simple Linear Elastic Calculations.....	12
2-3. Boundary Conditions Used for Stability Derivation .....	13
2-4. Stability Displacements .....	14
3-1. Percent of Plastic Moment and Drift from Low Yield Close Range.....	41
3-2. Percent of Plastic Moment and Drift from Medium Yield Close Range.....	42
3-3. Percent of Plastic Moment and Drift from High Yield Close Range .....	43
3-4. Percent of Plastic Moment and Drift from Low Yield Medium Range .....	44
3-5. Percent of Plastic Moment and Drift from Medium Yield Medium Range .....	45
3-6. Percent of Plastic Moment and Drift from High Yield Medium Range.....	46
3-7. Percent of Plastic Moment for Low, Medium, and High Yield Far Range.....	47
3-8. Drift for Low, Medium, and High Yield Far Range.....	47

## CHAPTER I

### INTRODUCTION

In recent years, much has been done in the field of blast analysis and design. Numerous papers and articles have been written on varying topics from proper application of blast loads to structural response. A major main point to glean from each paper is that the best way to mitigate blast damage or exposure is to increase the stand-off distance at which a charge can be placed. In most cases however, existing buildings do not have the capabilities to retrofit the buildings for further stand-off distances. Thus, it is critical to explore the response of structures to this extreme load case.

#### 1.1 BACKGROUND

Investigation into previous research completed on structural steel response to blast loading has uncovered several useful publications. Most of the publications have concentrated on the beam-column connections and column response. For the most part, there has been a joint forces technical manual for the basis of all blast case development. Multiple finite element modeling software packages have been used.

##### 1.1.1 Beam to Column Connections

Sabuwalla, Linzell, and Krauthammer (2004) discuss two types of connections, reinforced and unreinforced, used based on the American Institute for Steel Construction Northridge Moment Connection Test Program which are bolted-welded connections [1]. They note that the performance of the connections must be based on the performance of the steel frame; however, they also show that the reinforced connections do provide extra strength when subjected to blast loading. These reinforced connections have top and bottom cover plates located at the flanges of the connecting beam. These

reinforced connections perform correctly with their original purpose of forcing plastic hinges to develop away from the connection zone. To justify their stance, they use ABAQUS finite element models and evaluate the responses based on end displacements, rotations, and Von Mises stresses. The main failure points in the connections were near the weld access hole at the bottom of the beam and certain weld points. Each of these failures show only localized failure. They also noted that the TM5-1300 predicted higher values than that of their numerical models by almost 40%; thus the technical manual over-designs the beam [1].

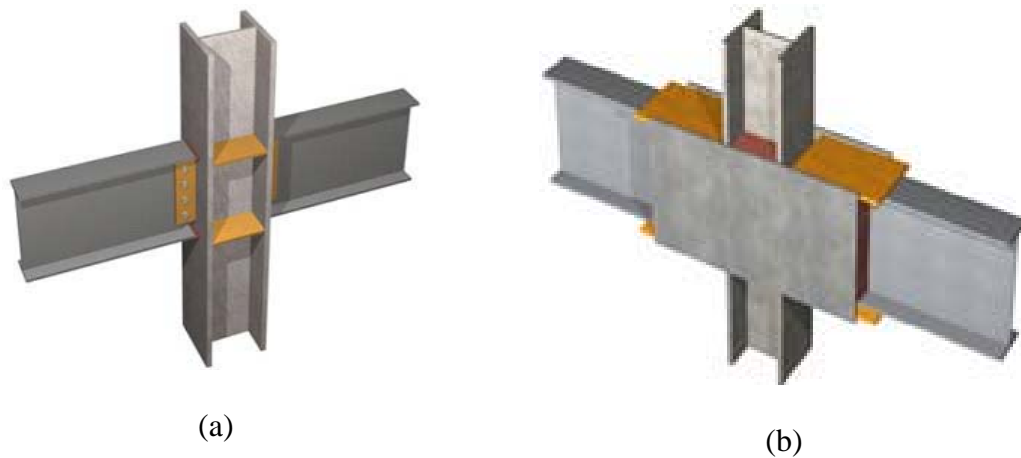


Figure 1-1: "Traditional" (a) and "Side Plate<sup>®</sup>" (b) moment connection systems [2]

Karns et al (2007) concentrated more on welded connections in the "GSA Test Program" [2]. The two types of connections tested were "Traditional" and "Side Plate<sup>®</sup>" moment connection systems as shown in Figure 1-1. These connections are also post-Northridge connections. The main difference in these two connections from the previous study was the "Side Plate<sup>®</sup>" connections had large plates on each side of the beam which would connect the outer edges of the top and bottom flanges together but does not touch the column. In this evaluation, LSDYNA and actual tests were used [2]. This test shows similar results in that the reinforced connection, the "Side Plate<sup>®</sup>" connection can produce

more pleasing result. Both connections survived the blast, but the "Side Plate<sup>®</sup>" connection showed improved post-blast capacity and the ability to absorb up to five times the external energy at first failure [2].

These two instances show that the connections are important, but the connection failures are typically local and do not dramatically affect the global performance in relation to the safety of the occupants. They also both prove that a reinforced connection of any type will prove to be a more blast resistant design.

### 1.1.2 Beam-Column Analysis

Lee, Kim, and Kim (2007) studied the local response of steel W-shapes to blast loading. They used computational fluid dynamics via LSDYNA as well. This study also concentrated on the weak axis of the columns. W14x211, W24x162, and W33x152 columns were tested. The W14 shape is considered a "typical" column while the other two are deep columns with equivalent strengths. Also considered were two different boundary conditions, fixed and pinned. This study showed several key results. First, the W14x211 column did not develop a plastic hinge at the midpoint under the tested blast load; therefore, the column would not lose its complete ability to support the dead load. However, the two deep columns were different. They did develop the plastic hinge, and this was accredited to the smaller weak axis moment capacity. The W33x152 showed damage in the flanges, so larger deformation and fracture is expected. As far as the boundary conditions response is concerned. They noted that the relative displacements of the fixed end were greater than the pinned case. However, the effective plastic strain follows an opposite trend. The pinned case showed increased damage [3]. Additionally this study shows that the deep column pinned cases would experience a fracture. It is

also noted that the relative web displacement is not always proportional to the strain [3].

Montalva, Godinho, and Marjanishvili (2008) considered the effect of axial load on a column's response to blast. In their study, they used only one column size, W14x176, and varied the axial load from zero to the buckling capacity of the column. The column was 15-ft tall with a 10-ft tributary width. Using a computer program called CONWEP, they developed uniform pressures to model the blast loading for their single degree of freedom models. For multi-degree of freedom models, they used DYNA3D using shell elements. Results were output in terms of peak displacement, rotation, and ductility [4]. They concluded that multi-degree of freedom models were more accurate especially when the axial load increased to about 20% of the critical value. Collapse was reached when the axial load increased to 60% of the buckling capacity (Figure 1-2).

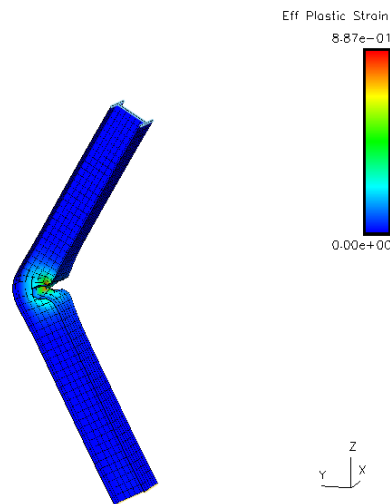


Figure 1-2: DYNA3D Results for 60% Axial Load subjected to Blast [4].

### 1.1.3 Frame System Analysis

Hwang and Anderson (2008) compiled a conference paper in 2008 entitled "Response of a Low Rise Steel Building to Air Blast." In this study, they compared the response of the 3-D frame to the parameters set by the Uniform Building Code 1994

using interstory drift as a guideline for response [5]. The steel frame designed was designed using the 1994 Uniform Building Code with 13-foot floor heights and six 30-foot bays in the longitudinal direction and four 30-foot bays in the transverse. Floor slabs were designed to be concrete with metal decking. After the design, a SAP2000 Version 9 model was generated, and the default settings were used for plastic hinges [5]. Standard ASTM A572 Gr.50 steel was used, and all the column bases were assumed to be fixed. Again in this work, CONWEP was used to develop the blast load cases. Assuming, uniform pressure, three load cases were developed; however, only two cases were discussed. For the case of 1000 lbs at 15 feet standoff, it is noted that the beams only have small plastic rotation, therefore, the building is considered safe according to the standards in FEMA356 [5]. The other case discussed was 2000 pounds at 20 feet. In this case, the columns in the first floor are considered to have critical damage as their plastic rotation is higher. With these results, the interstory drift was calculated for each case and compared to the limitations set forth by the UBC as seen in Figure 1-3 [5]. This also shows that the larger case exceeds safe parameters. Also noted in this paper is that the demand to capacity ratio is higher in the strong axis columns.

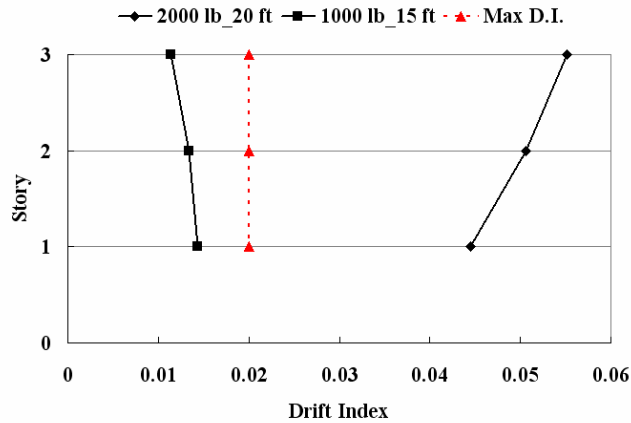


Figure 1-3: Drift Ratios for Each Major Blast Case Studied [5]

## 1.2 MOTIVATION

As seen, numerous studies have been conducted within the realm of blast loading and steel structures. However, there has yet to be anyway to relate each category to each other. Thus it is important to investigate the column response individually then use these results to better interpret the results from the three-dimensional frame model. In Chapter 2, the column capacity analysis will be explained in depth and response will be studied. The three-dimensional frame will then be explored in Chapter 3 for its response to specific blast load cases, and using the column results, the frames damage level and consequently the frames response can be determined. This case is explored for the case in which the building meets current building code and is designed for a multi-hazard exposure.

## CHAPTER II

### COLUMN CAPACITY ANALYSIS

#### 2.1 Background

During a blast event, columns are often the most directly affected elements in a structure. Thus, an investigation into the response of columns is needed. In this study, W8x31 members were chosen from a design of a 3-story frame with 12 foot story heights using the International Building Code 2006 as discussed in the following chapter. Only a single column was chosen in the design for the largest loading case, interior lower level. The column was then used for all columns in the frame. This may contribute to a possible over-design; however, the assumption was made that this could be a realistic scenario for ease of construction. The column models were developed using Computers and Structures, INC.'s SAP2000 software. This software was chosen for its ability to perform nonlinear fiber modeling. Versions 12 and 14 were utilized.

#### 2.2 Column Models

The material used was the standard ASTM A572 Grade 50 steel as provided by the software. Also the software is able to select the section size based on the American Institute for Steel Construction's Steel Construction Manual 13<sup>th</sup> Edition [6]. Therefore, the W8x31 section size was available through the program as well.

As stated, the column models were developed in SAP 2000 as nonlinear fiber models. The locations of the fibers were "User Defined." As determined from multiple simulations, the user-defined option was more accurate than the default number and

locations. The default locations only allowed for a single fiber in the web which cause and inaccuracies in the simple linear elastic runs. After increasing to two fibers in the web, the results were calculated to six percent accuracy. Figure 2-1 shows location of the fiber elements. The location of the fiber hinges were a distance of 0.1 feet relative to the distance from the plastic hinge location on either side of the plastic hinge location. This allowed for tracking of not only the eight fibers but also in two different locations adjacent to the plastic hinge location. These settings were used by referencing previous study in reinforced concrete column by Tadepalli (2009) [7].

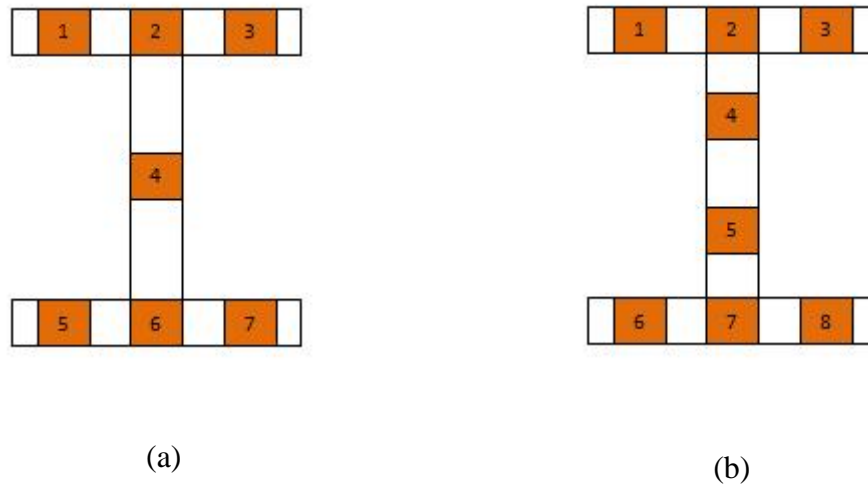


Figure 2-1: Default (a) vs. User-Defined (b) Fiber Locations

There were three different boundary conditions considered. Pinned-Roller, Fixed-Free Rotation, and Fixed-Fixed Rotation were used in order to model a more realistic boundary condition. These boundary conditions were set using the restraints option available in the software which allows for releasing translational or rotational degrees of freedom in three directions [8]. The column was checked to ensure that the major axis was the line of action for the lateral load.

## 2.3 Analysis

For the analyses of the columns, numerous models were run in order to verify the model as well as extract the needed results. Each of the three boundary conditions was run with and without an axial load for a total of six column model runs.

### 2.3.1 Load Development

A displacement-controlled load case was developed for the lateral load while the axial and dead loads were also applied. The axial load was applied as a point load at the top joint of the model. The magnitude of this load was determined using the three story frame design which will be discussed in the following chapter. The dead load was the default application used by SAP2000. This dead load, or self-weight load, is a force that is distributed along the length of a member with a magnitude of the weight density multiplied by the cross-sectional area. This load is set to a default application in the global negative "Z" direction [8].

The lateral load, as mentioned before, was an applied displacement at the location of where the plastic hinge should form. The displacement applied is a unit displacement that is incremented to some limitation or until there are convergence issues. The displacement was used as the applied load since an applied force will cause convergence issues as the model works its way further out the force-displacement curve as initial weakening occurs. Thus using the displacement-controlled loading, the model can be taken through the entire curve which allows the performance of the column to be monitored throughout its usefulness.

### 2.3.2 Model Cases

Each boundary condition, pinned-roller, fixed-free rotation, and fixed-fixed

rotation, was chosen to accurately incorporate axial load effects. Each model was identical in all other properties to including fiber locations. Figure 2-2 shows the three end conditions chosen.

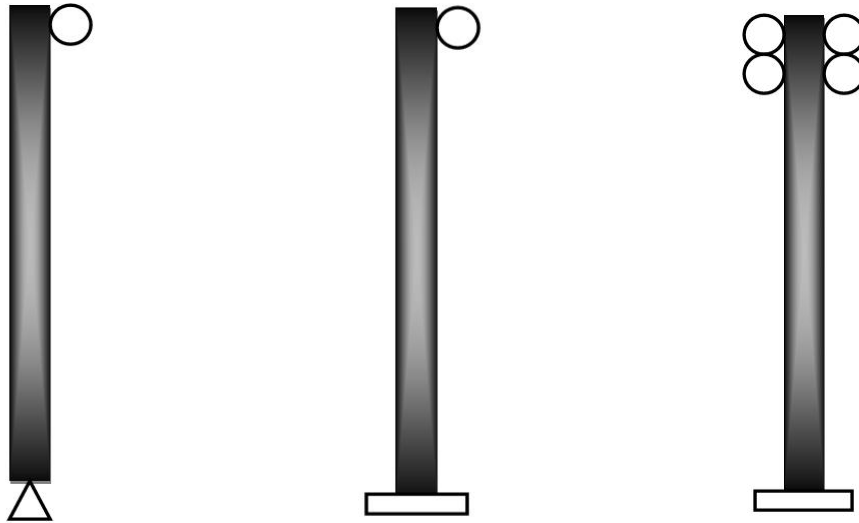


Figure 2-2: Column Models Used (Sketch) was (L to R) Pin-Roller, Fixed-Free Rotation, and Fixed-Fixed Rotation.

## 2.4 Analytical Calculations

A range of analytical solutions were explored in order to monitor the computer model responses and determine appropriate damage levels.

### 2.4.1 Elastic Response

The first calculations to be conducted were that of the elastic response with a proposed blast pressure. This was calculated using the formulation shown in the AISC Steel Construction Manual [6]. The negatives to using this approach are that it does not include an axial load and is dependent upon the value of the distributed load. For this reason, the load case used was for median standoff distance and charge weight. Also considered in this calculation was the application of the load weather to use a uniformly distributed or point load. Therefore, both calculations were completed in order to have a

comparison. The uniformly distributed load cases were Case 1 for simply supported, Case 12 for fixed-supported, and Case 15 for fixed-fixed [8]. Similarly for the concentrated load case, Case 7 for simply supported, Case 13 for fixed-supported, and Case 16 for fixed-fixed [8]. Each calculation revealed a maximum moment and deflection that can be compared other results. Table 2-1 shows the results from these calculations.

Table 2-1: Results from Elastic Calculations from AISC Manual

From AISC Manual				
	$M_{max}$ (kip-ft)	$M_{max}$ (kip-in)	$\Delta_{max}$ (ft)	$\Delta_{max}$ (in)
<b>Fixed-Supported</b>				
<b>12 Distributed</b>	1451.52	17418.24	0.408	4.90
<b>13 Center</b>	2177.28	26127.36	0.703	8.44
<b>Fixed-Fixed</b>				
<b>15 Distributed</b>	967.68	11612.16	0.197	2.36
<b>16 Center</b>	1451.52	17418.24	0.393	4.72
<b>Simple Beam</b>				
<b>1 Distributed</b>	1451.52	17418.24	0.983	11.794
<b>7 Center</b>	2903.04	34836.48	1.573	18.871

Simple linear elastic calculations were completed as well to show the load at first yield as well as the displacement. These calculations were based on the maximum moment being the sum of the yield strength,  $F_y$ , times the elastic section modulus,  $S$ . These results are tabulated in Table 2-2 below.

Table 2-2: Simple Linear Elastic Calculations

Linear Elastic Analysis		
<b>F<sub>y</sub> (ksi) =</b>	50	
<b>S (in<sup>3</sup>) =</b>	27.5	
<b>M<sub>max</sub> (kip-in) =</b>	1375	
	<b>W<sub>1stYield</sub> (kip/in)</b>	<b>Δ<sub>max</sub> (in)</b>
<b>Fixed-Fixed</b>		
<b>Distributed</b>	0.796	0.279
<b>Center: P (kips) =</b>	76.389	0.372
<b>Simply Supported</b>		
<b>Distributed</b>	0.530	0.929
<b>Center: P (kips) =</b>	38.194	0.745

### 2.4.2 Elastic Buckling

The elastic buckling calculations for this case were also considered for three separate boundary conditions. The model sketch in Table 2-4 shows a sample model for these calculations. For the derivation of these calculations, Theodore Galambos and Andrea Surovek's book, Structural Stability of Steel, was used [9].

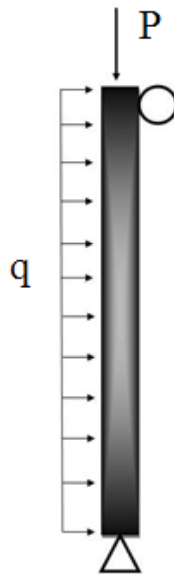


Figure 2-4: Column Model Sketch for Buckling Response Verification

To start the analytical solution, we begin using the simple flexural differential equation below.

$$EI_x v^{iv} + P v'' = q$$

Where  $E$  is the modulus of elasticity,  $I_x$  is the moment of inertia about the x-axis,  $P$  is the distributed lateral pressure,  $q$  is the axial load, and  $v$  is the displacement [9]. Solving the differential equation using the boundary conditions shown below, Table 2-3, the displacement at any location can be shown as

$$v = \frac{q}{Pk^2} \left[ \left( \frac{1 - \cos(kL)}{\sin(kL)} \right) \sin(kz) + \cos(kz) + \frac{(kz)^2}{2} - \frac{k^2 Lz}{2} - 1 \right]$$

where  $v$  is displacement,  $P$  is distributed lateral load,  $L$  is total length,  $z$  is location along the member. The equation

$$k^2 = \frac{P}{EI}$$

is used to describe the  $k$  term [9]. The maximum deflection is located at the mid-span thus

$$v\left(\frac{L}{2}\right) = \frac{q}{Pk^2} \left( \frac{1}{\cos\left(\frac{kL}{2}\right)} - \frac{(kL)^2}{8} - 1 \right)$$

This can then allow the elastic deflection for a simple case with one of the blast loads calculated for the 3-D frame to be used to verify the model. This was proven in the book.

Table 2-3: Boundary Conditions Used for Stability Derivation [9]

	$v(0)$	$v(L)$	$v'(0)$	$v'(L)$	$v''(0)$	$v''(L)$
<b>Simply Supported</b>	0	0	-	-	0	0
<b>Fixed-Fixed</b>	0	0	0	0	-	-
<b>Pinned-Fixed</b>	0	0	-	0	0	-

Upon completion of the derivation, the equations below were developed for each boundary condition.

$$v = \frac{-lqz}{2p} + \frac{qz^2}{2p} + \frac{lq * \cot(\frac{kl}{2})}{2kp} + \frac{lq * \cos(kz) * \cot(\frac{kl}{2})}{2kp} + \frac{lq * \sin(kz)}{2kp}$$

for the fixed end, and

$$v = \frac{-q}{k^2p} + \frac{qz^2}{2p} + \frac{q * \cos(kz)}{k^2p} + \left[ \frac{q}{2kp} \left( \frac{-2 + (2 - k^2l^2) * \cos(kl) + 2kl * \sin(kl)}{kl * \cos(kl) - \sin(kl)} \right) \right] z + \left[ \frac{q}{2k^2p} \left( \frac{2 + k^2l^2 - 2 * \cos(kl) - 2kl * \sin(kl)}{kl * \cos(kl) - \sin(kl)} \right) \right] \sin(kz)$$

for the pinned-fixed case. The latter two cases are shown in the Table 2-4 were the same as discussed in a later chapter.

Table 2-4: Stability Displacements

Displacements from Derived Equations		
	Displacement (ft)	Displacement (in)
<b>Pinned-Fixed</b>	0.439	5.27
<b>Fixed-Fixed</b>	0.204	2.45
<b>Simply Supported</b>	0.233	2.80

### 2.4.3 Plastic Analysis

Plastic analysis calculations are the next set of analytical work to be completed. Two separate conditions were derived for this case, one with the plastic region only in the flange and the other with the plastic region in the flange and web. These calculations were derived using B.G. Neal's The Plastic Methods of Structural Analysis and James M. Gere's Mechanics of Materials 6<sup>th</sup> Edition [10, 11]. The

curvature and displacement formulations below are specifically for the W8x31 section size used throughout this work.

This method first begins with developing a moment equation for the section.

The equation for plastic only in the flange is as follows:

$$M = \frac{1}{24} \left[ 4Ek(h - 2t_f)^3 t_w + 3b_f F_y (h - 2z)(h + 2z) + 8b_f Ek \left( (b_f - h)^3 + z^3 \right) \right]$$

where  $k$  is the curvature,  $z$  is the distance from the neutral axis to the plastic region,  $E$  is the modulus of elasticity,  $h$  is the height of the section,  $t_f$  is the thickness of the flange,  $t_w$  is the thickness of the web, and  $b_f$  is the width of the flange. Figure 2-5 shows two cases, plastic in the flange only and plastic in the flange and web.

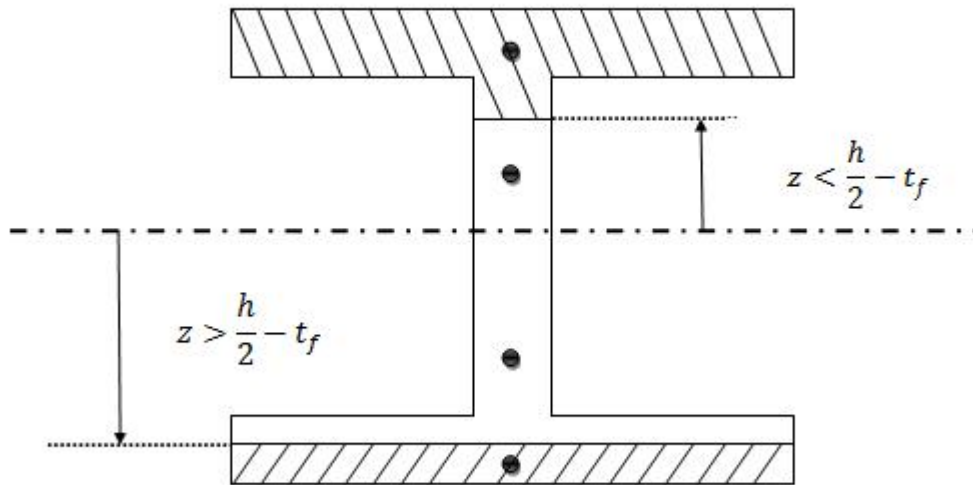


Figure 2-5: Plastic in the Flange and Web (top) and Plastic in the Flange Only (bottom)

The curvature can then be found by substituting,  $0.5 \cdot P \cdot x$ , into the moment equation. The curvature is then

$$k = \frac{-(1E^{-3}) + 0.5k_yPx + (6.27E^{-5})z^2}{8((1.95E^{-2}) + (3.03E^{-3})z^3)}$$

and substituting back into the equation

$$k_y = \left(\frac{f_y}{E}\right)\left(\frac{S}{I}\right)$$

where S is the elastic section modulus. The displacement can be found by integrating the curvature equations with respect to  $x$ , the position along the member,

$$\Delta = -0.00641x + 0.000689Px^2$$

where  $x$  is the location of the displacement and  $P$  is the load applied.

The next derivation was for the plastic region into the web. With this parameter, the moment equation was

$$M = \frac{1}{2}b_fF_y(d - t_f)t_f + \frac{1}{6}Ekt_wz^3 + \frac{1}{8}f_yt_w(d - 2(t_f + z))^2$$

where again  $k$  is the curvature and  $z$  is the distance from the neutral axis to the plastic region. For this case, the curvature is found to be described in the equation below.

$$k = \frac{168.539Ik_y \left( -\frac{0.0172b_f d^2 f_y}{EI k_y} + 0.5Px - \frac{0.0045b_f f_y (d - 2(0.036d + z))^2}{EI k_y} \right)}{b_f z^3}$$

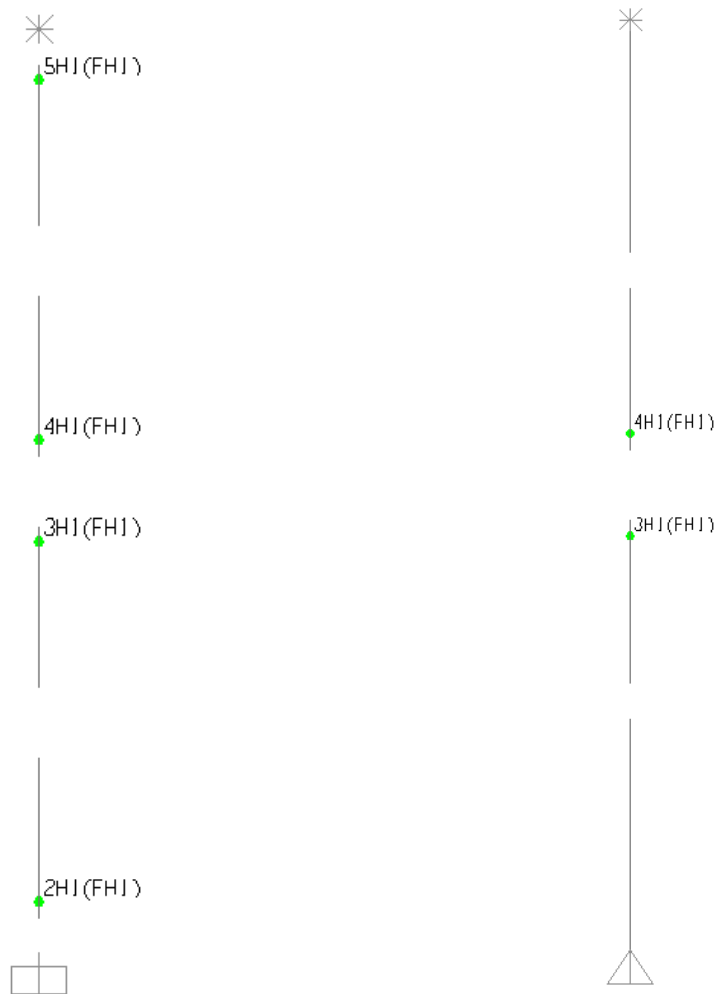
After the same process as previously mentioned, the deflection equation can be shown as

$$\Delta = \frac{x(-0.391 + 0.250Px + 0.038z - 0.005z^2)}{z^3}$$

Where  $x$  is the position along the member and  $z$  is the location from the centroid to the plastic region. This shows that as  $z$  approaches zero, the displacement would go to infinity which demonstrates a plastic hinge formation. Therefore, a fully plastic moment can be calculated in order to show at what point in time the plastic hinge is forming in the SAP2000 models. Note that the fully plastic moment is 1551.41 kip-in.

## 2.5 Computer Models Analysis

Three separate SAP 2000 models were evaluated to determine the columns resistance to a lateral load. Each model was exactly identical except for the boundary conditions, and the fixed-fixed case also had two extra fiber hinge locations due to the concentrated moments near the end restraints. Each model includes the effects of P- $\delta$  in order to more accurately incorporate the axial load. Figure 2-6 shows each modeled case with the location of the fiber hinges.



2-6: Location of Fiber Hinges for Fixed-Fixed (left) and Other Two Cases (right)

The fixed-fixed case had the best performance of the group. The displacement limitation for this case was six inches although the column cannot support that level of displacement. After the run, it showed satisfactory Force-Ductility and Moment-Rotation Curves. From these plots, the critical states can be located, and the performance evaluated. Each grid point is a step that has been calculated by SAP2000. These plots are listed below in Figure 2-7 and 2-8. The last data point in the Force-Ductility curve does show the ductility at which the plastic hinge is formed. This can be determined by referencing the same grid points associated with the Moment-Rotation curve. The Moment-Rotation Curve has been normalized to the plastic moment previously calculated in this chapter. The column has, however, reached a limit at which its load carrying capacity is deteriorating at a rapid rate. Therefore, it has been determined at exactly what force on the member allows for this displacement, and an assessment is made in the next chapters as to the damage levels of the columns on the building's exterior face when subjected to the blast pressures. The force at which the plastic hinge develops is 10.78 kips/ft. Below this value, the column can still support a considerable load and be relatively safe for occupants. This shows that first yield in this member will occur around 6.5 kips/ft which is the point at which the column will begin to lose its load carrying capacity. The range is then set for the column response with these end conditions. Between 6.5 kips/ft and 10.78 kips/ft, damage is occurring and the column is weakening. Beyond 10.78 kips/ft, the column will become unstable. Below 6.5 kips/ft, the column will be relatively unharmed with relation to its load carrying abilities.

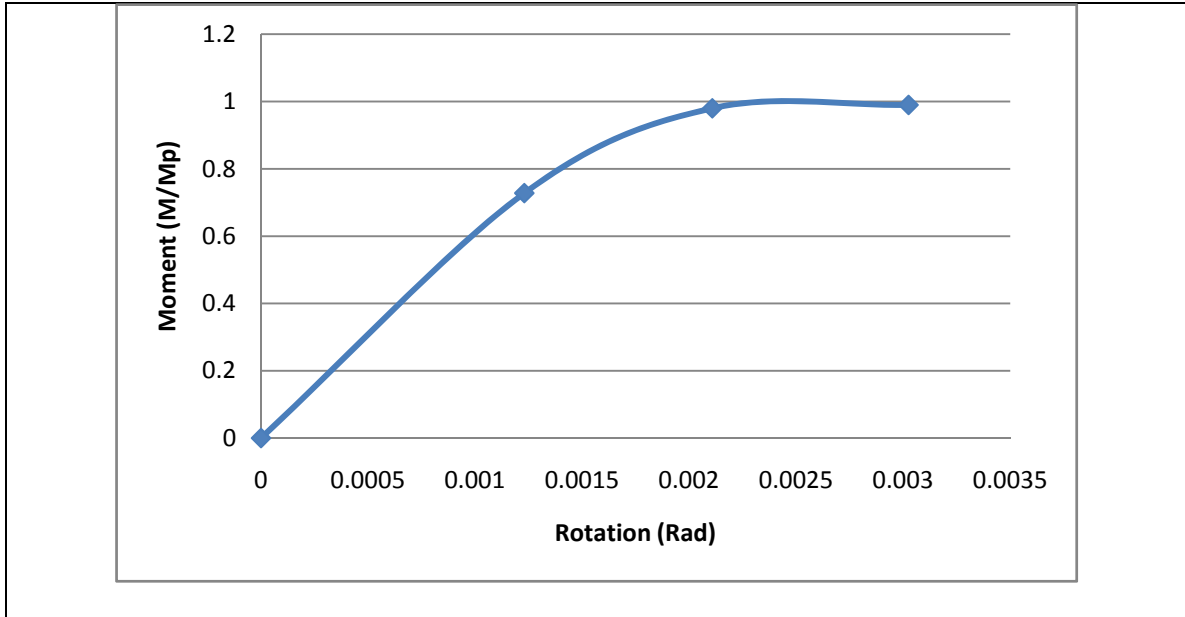


Figure 2-7: Moment-Rotation Curve for Fixed-Fixed Rotation

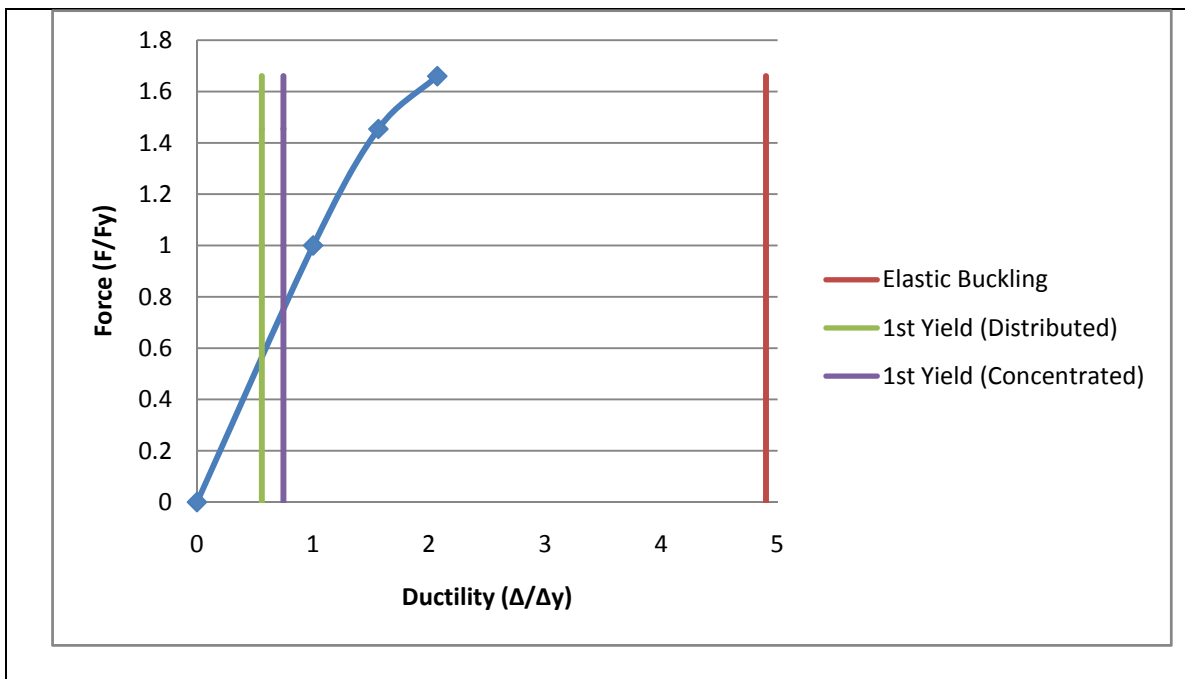


Figure 2-8: Force-Displacement Curve for Fixed-Fixed Rotation

Attempts were made to analyze the other two boundary conditions, Fixed-Free Rotation and Pinned-Free Rotation, but the results did not reach any of the calculated values for first yield, elastic buckling, or plastic moment. The results from these cases can be seen in the Appendix. Consequently, the results from the Fixed-Fixed

Rotation case were used to assess the damage to the three-dimensional frame in the following chapter.

## CHAPTER III

### MULTI-HAZARD STEEL FRAME ANALYSIS

#### 3.1 Background

The previous chapter was dedicated to the response of columns to lateral loading. With these results, we can assess the response of the three dimensional frame subjected to a large lateral load, specifically blast. The usage of the damage states pointed out in the previous chapters allows the evaluation of column damage levels throughout the structure. This grants the ability to assess in greater detail the reliability of the damage structure in order to determine the resistivity of this particular frame to blast loading.

#### 3.2 Design

In order to have an accurate depiction of an in-service building, location, function, and size had to be estimated. The location chosen was Oxford, Mississippi, due to the prominence of a Federal Courthouse and other key Federal facilities. Upon drive-by inspection, the buildings appear to be low rise with relatively large span lengths. Therefore, a design building would have 3 stories with 20 foot by 40 foot bays with three 40 foot longitudinal bays and two 20 foot bays through the depth. The location of Oxford is also significant in that it is in a true multi-hazard location. It is located approximately 150 miles from the southern tip of the New Madrid fault and approximately 280 miles from the Gulf of Mexico Coast. This exposes this location to not only severe winds but also earthquake. The International Code Council's International Building Code 2006 (IBC) was used to develop all design loads and was followed throughout the entire design

process [12]. The three-dimensional model to be depicted in the sketch in Figure 3-1 which also contains floor slabs.

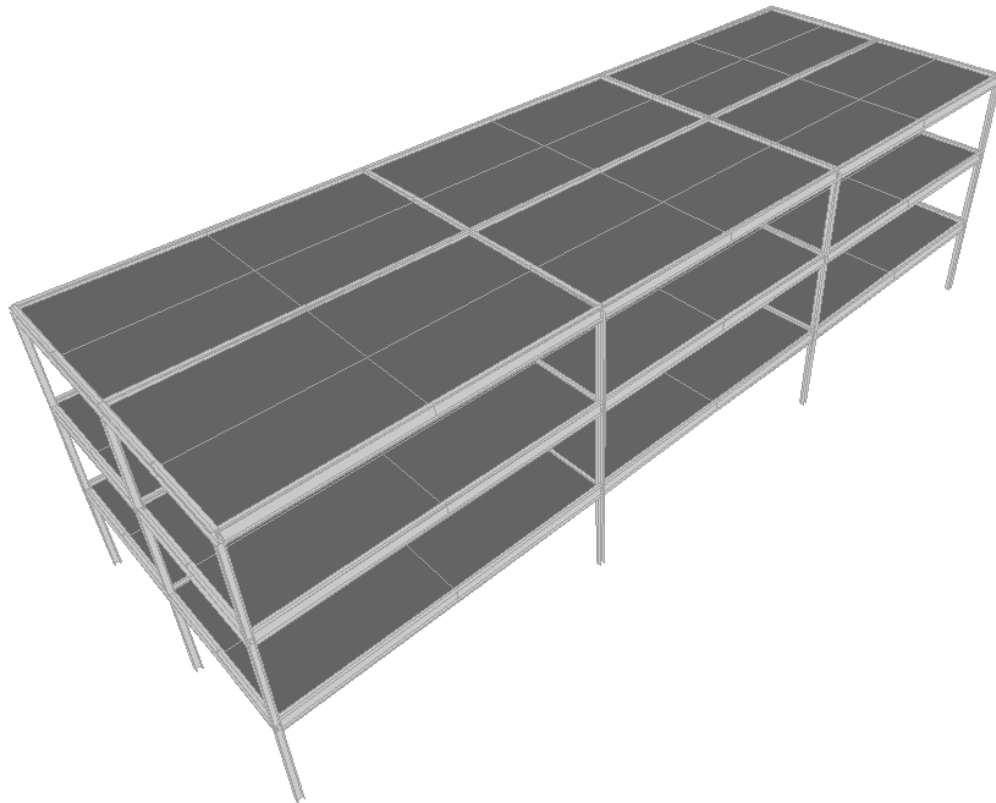


Figure 3-1: 3-D Frame Sketch

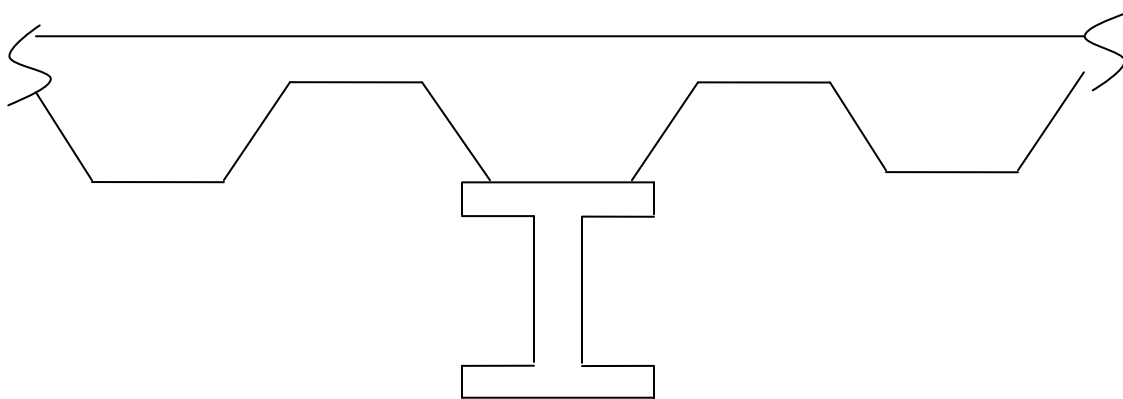


Figure 3-2: Composite Slab Sketch

### 3.2.1 Slab Design

To begin the design process, the floor slabs were developed first. The slabs are composite concrete with steel decking. The live load used was the IBC and ASCE/SEI 7-05 recommendation for “Office Use” which is 50 pounds per square foot and the roof load was 20 pounds per square foot which is the recommendation for an “Ordinary Flat” roof. From these basic loads, ACI 310-05 was referenced for the composite slab design [14]. A three-inch slab with 1/8 inch steel plate with 3.5 inch spans was used for the slab. Figure 3-2 shows a simple sketch of the floor slab system.

After developing a series of load cases using the Load and Resistance Factored Design specifications mentioned in Chapter 16 of the IBC which is extracted from ASCE/SEI 7-05, the largest load case was chosen which was

$$1.2DL + 1.6LR + f_1LL$$

where  $DL$  is dead load,  $LR$  is the roof live load, and  $LL$  is live load [12, 13]. The  $f_l$  factor is assumed to be 1 for “floors in places of public assembly.” This was chosen due to the federal buildings having large meeting areas and courtrooms. Also, this allows for a more conservative design. With these calculations complete, the composite beam section can be selected.

### 3.2.2 Composite Beam Design

The composite beam selection was completed by using the AISC Steel Construction Manual 13<sup>th</sup> Edition and Structural Steel Design by Jack C. McCormac [8, 15]. First the required moment strength was calculated followed by an assumed value for

$\alpha = 1$  and the calculation of  $Y_2$ .  $Y_2$  was figured using 3 inch slab thickness which was 2.625 inches. A W18x50 beam was selected from Table 3-19 in the AISC Manual, and  $Y_1$ ,  $\sum Q_n$ , and actual  $\alpha$  and  $Y_2$  are given. The actual  $Y_2$  is 2.875 inches. This requires an interpolation between  $Y_2$  values of 2.5 and 3 to show that the ultimate moment is less than the ultimate moment value of the W18x50 section [8]. The column design follows now that the beam and slab design was complete.

### 3.2.3 Column Design

Proper column design is critical not only in a realistic setting but also for this research since the response of the 3D frame is based off of column response. The steps followed for column design are located in the McCormac text mentioned before as well as Steel Structures: Behavior and Design 5<sup>th</sup> Edition by Charles G. Salmon, John E. Johnson, and Faris A. Malhas [15, 16]. First, the load on the top floor was calculated which was determined to be 109.5 kips. The load is followed by determining the appropriate value for K which is determined using the AISC Manual in the Specifications Chapter C Table C-C2.2 [6]. The theoretical K value is 1 for this case; therefore the value of KL is equal to 12. After determining load and theoretical KL value, Table 4-1 from the AISC Manual is used to determine a section size that can support the axial load with the appropriate KL value [6, 15]. Once a section size is selected, W8x31 for this case, calculations are completed to ensure that it is an appropriate size. The cross-sectional area and  $r_y$  values are used to calculate multiple factors to include the following:  $[KL/r]_y$ ,  $F_e$ ,  $F_y/F_e$ ,  $F_{cr}$ ,  $\Phi F_{cr}$ , and  $\Phi P_n$  [15]. This allows for a comparison of  $\Phi P_n$  to  $P_u$  and the actual cross-sectional area to the required area. The comparison of  $\Phi P_n$  to  $P_u$  shows that the W8x31 section is only being used for 30% of its capacity. As a result, the actual

area is 3 times greater than the required area. The W8x31 is the smallest rolled section available in the AISC Manual [8]. This is followed by the same procedure to determine a section size needed for the lower level columns. The first floor or lowest level was calculated, and the W8x31 section was also used. At the lower level, the column was using 75% of its capacity. The W8x31 section size was determined to be effective for use through the entire three-story three-dimensional frame. To relate this back to a practice design-build, it was assumed to use the same section size for all columns in the frame. This was also check for three locations along the first story, interior, side, and corner and was shown to be effective. Figure 3-3 shows the W8x31 section with labeled dimensions.

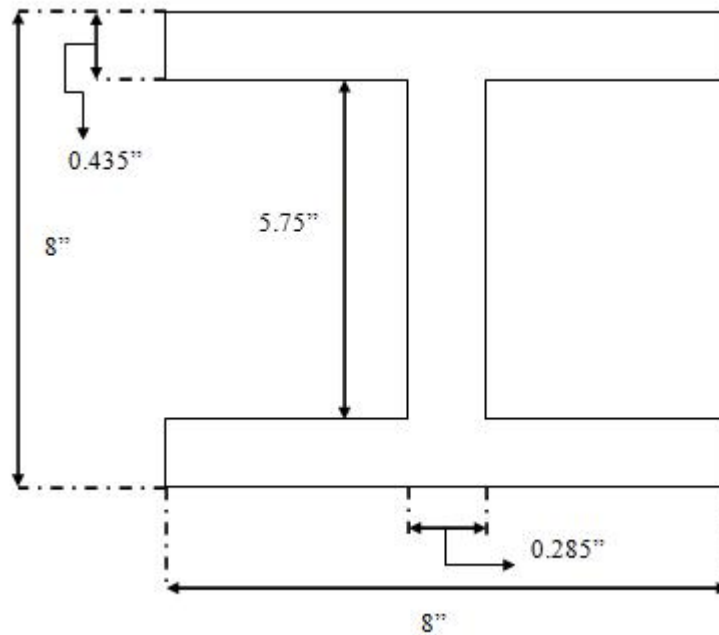


Figure 3-3: W8x31 Dimensions

### 3.2.4 Seismic Design

Due to the selected location of the design, a seismic load case must be developed and tested against the frame to determine effectiveness. According to the IBC 2006 and ASCE/SEI 7-05, the seismic design load is calculated as a static equivalent; however, it is obvious that a true seismic load is dynamic [12, 13]. Thus an investigation was completed to determine the effectiveness of the static equivalent compared to a more realistic dynamic result.

First the development of the static equivalent case in order to complete the design procedure was completed with “CodeMaster: Seismic Design” by Structures & Codes Institute which gives a step-by-step procedure for the process [17]. The spectral response accelerations  $S_s$  and  $S_1$  are first determined.  $S_s$  and  $S_1$  are applicable for short periods and for a 1-second period and are determined using an internet tool provided by the United States Geological Survey which allows the input of the particular building code used and zip code of proposed location, and the USGS code will output the spectral response accelerations [18].  $S_s$  and  $S_1$  for Oxford, Mississippi are 0.53 and 0.175, respectively. The seismic design classification, or SDC, follows next. The SDC is based on the use of the building and the type of soil at the location. For the current application, site class “D” is used which is used to determine two site coefficients,  $F_a$  and  $F_v$  [12].  $F_a$  and  $F_v$  are 1.376 and 2.1, respectively. The 5-percent-damped design spectral response acceleration for short periods and 1-second periods are then calculated using the following equations.

$$S_{DS} = \frac{2}{3} F_a S_s$$

$$S_{D1} = \frac{2}{3} F_v S_1$$

After these are determined, an occupancy category is chosen. Occupancy Category II was chosen with  $S_{DS}$  of 0.486 and  $S_{D1}$  of 0.245 as a basis [13]. This category is generalized due to this structure not falling under the other three categories which have more specific guidelines. Now with the preliminary coefficients available, the design category is chosen. This structure can be designed under design category “C” or “D” with “D” being the more conservative approach. “D” was chosen [13]. Therefore, the fundamental period is calculated using

$$T_a = C_t h_n^x$$

where  $C_t$  and  $x$  are period parameters from ASCE/SEI 7-05 Table 12.8-2 and  $h_n$  is the height in feet above the base to the highest level of the structure.  $C_t$  and  $x$  were chosen for a steel moment-resisting frame which constitutes  $C_t$  to equal 0.028 and  $x$  to equal 0.8 [13]. A check is then completed to show that the fundamental period is not greater than the product of the coefficient for upper limit on the calculated period,  $C_u$ , and the approximate fundamental period,  $T_a$ .  $C_u$  is found from Table 12.8-1 in ASCE/SEI 7-05 to be 1.4 [13].  $T_{max}$ , which is the product of  $C_u$  and  $T_a$ , is resolved to be 0.689 which is less than  $T_a$  which is 0.492 therefore this check is complete.  $T_s$  is the next check to be completed.  $T_s$  is the period at which the flat portion of the response spectrum transitions to a descending value and has a typical value of 0.5.  $T_s$  is shown in Figure 3-4 which is extracted from ASCE/SEI 7-05.

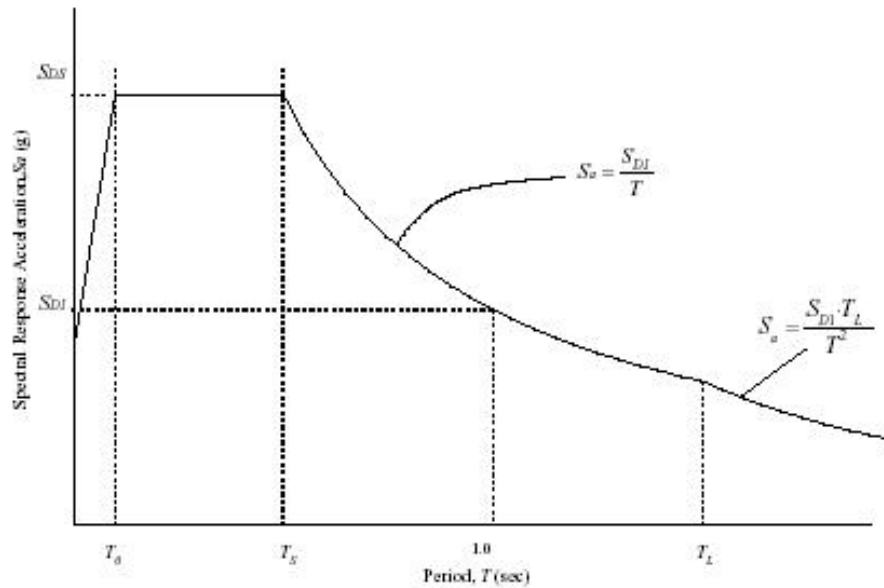


**FIGURE 11.4-1 DESIGN RESPONSE SPECTRUM**

Figure 3-4: Design Response Spectrum from ASCE/SEI 7-05 Figure 11.4-1[13]

This is calculated by dividing the spectral response acceleration for 1-second periods,  $S_{DI}$ , divided by the spectral response acceleration for short periods,  $S_{DS}$ , which is determined to be 0.504. A dynamic analysis may be required for three story buildings if the period is greater than 3.5 times  $T_s$ .  $3.5T_s$  is equal to 1.764 which is less than  $T_a$  of 0.492 therefore the linear static analysis is efficient and can be continued. The next two factors to resolve are the response modification coefficient,  $R$ , and the seismic importance factor,  $I$  [13]. The response modification factor is dependent upon the type of system being designed, and the seismic importance factor depends on the occupancy category. From Table 12.2-1 and Table 11.5-1 in ASCE/SEI 7-05,  $R$  and  $I$  are shown to be 2 and 1 respectively [13]. The first process in developing the total base shear is calculating the seismic response coefficient,  $C_s$ .  $C_s$  is resolved in the equation

$$C_s = \frac{S_{DS}}{\left(\frac{R}{T}\right)}$$

which has a value of 0.243.  $C_s$  is then multiplied by the total weight of the building plus any contents permanently attached to the building,  $W$ , to determine the total base shear,  $V$ . The total base shear is then distributed to each floor, or the location of concentrated masses, by the following equation.

$$F_x = C_{vx}V$$

where

$$C_{vx} = \frac{w_x h_x^k}{\sum_{i=1}^n w_i h_i^k}$$

The equation for  $C_{vx}$  can be described in Figure 3-5. The coefficient  $k$  depends on the value of the period. For the current case,  $k$  of 1 was used [17]. With the base shear distributed through the height of the structure, those values can then be distributed throughout the depth. Figure 3-6 shows the seismic forces distributed throughout the three-dimensional frame. After a check, the frame is sufficient with the earthquake loading. The base reactions in the SAP model were 170.58 kips compared to the calculated 168.45; therefore, the model is performing properly and can be used for the remaining analysis.

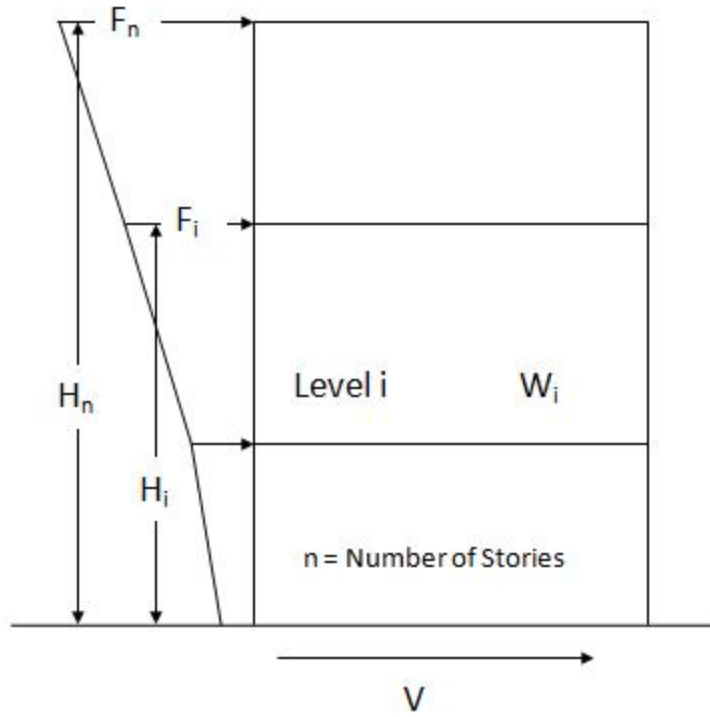


Figure 3-5: Distribution of Total Base Shear [17]

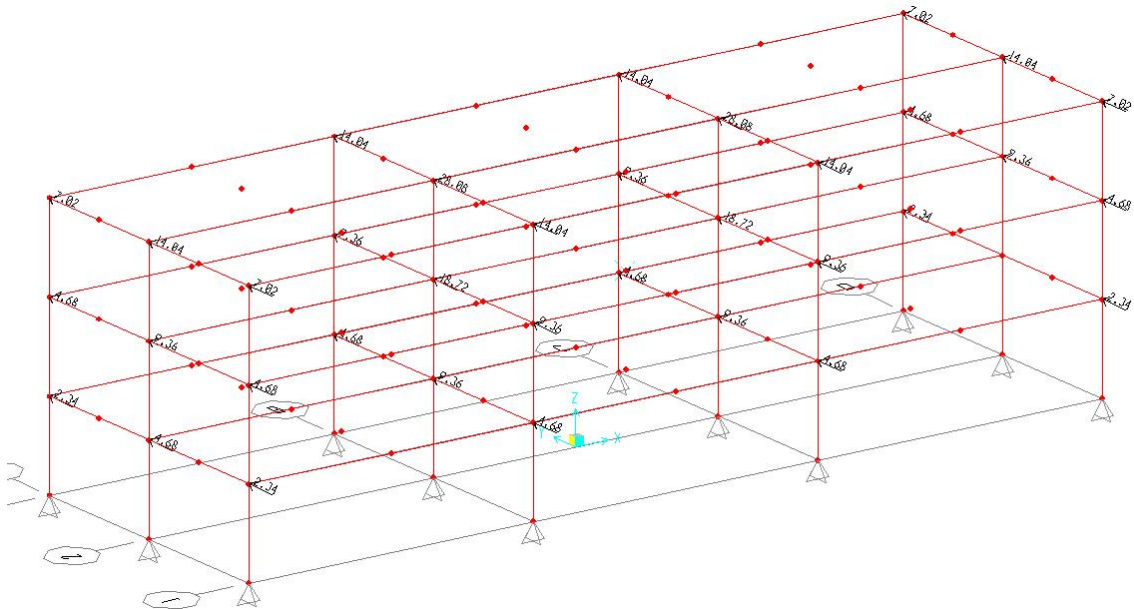


Figure 3-6: Base Shear Distributed Throughout the 3D Frame

True seismic loading, however, is actually a dynamic load. It is an applied acceleration to the base of the structure. For ease of analysis, the three dimensional frame designed was modeled as an equivalent 2-D frame. In this frame, one of the transverse frames was used; Figure 3-7 shows the equivalent 2-D model with two 20 foot bays and 3 stories high. The beams were converted to equivalent sections in order to more accurately represent the stiffness of the structure and the effects of the slab. This conversion was done by utilizing the “General Section” under “Frame Sections” in SAP2000.



Figure 3-7: Equivalent 2-D Frame for Dynamic Analysis

The dynamic analysis for earthquakes is highly dependent upon the time history function. For this instance, SAP2000 has several default time history functions available [7]. The function chosen to use was “holliste-1.” It is assumed that this function is based on the 1989 earthquake that measure 6.9 on the Richter scale in Hollister, California. The time history plot is shown below in Figure 3-8 directly from SAP2000.

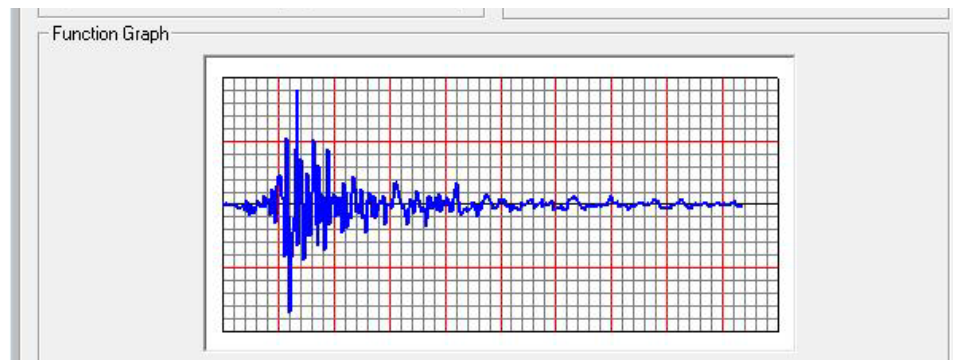


Figure 3-8: Time History Function for Earthquake Analysis [7].

This time history plot gives accelerations that are applied to the frame at its base in order to accurately depict the seismic event. After the model has been tested, the base reaction and intra-story drift were calculated. The base reaction for this case was calculated to be only 57.325 Kips which is considerably less than the static base shear calculated.

Therefore, the static case is a much more conservative approach for this scale of an earthquake. As for the intra-story drift, the drift index calculated was 0.014 which is less than the 0.02 allowed by code [12]. Therefore the frame is acceptable and was able to carry the dynamic loading.

### 3.2.5 Blast Loading

Blast loading is similar to seismic in many ways, but they are also different. Blast and seismic are similar in that they are both applied as a lateral force on a structure.

Typically, buildings designed for seismic loading have some resistance to blast. The magnitudes, however, can have major differences. A blast pressure wave is a function of the charge weight of equivalent TNT and standoff distance. Figure 3-9 shows a diagram from the joint service technical manual, TM5-1300 [19]. TM5-1300 is the manual entitled “Structures to Resist the Effects of Accidental Explosions.”

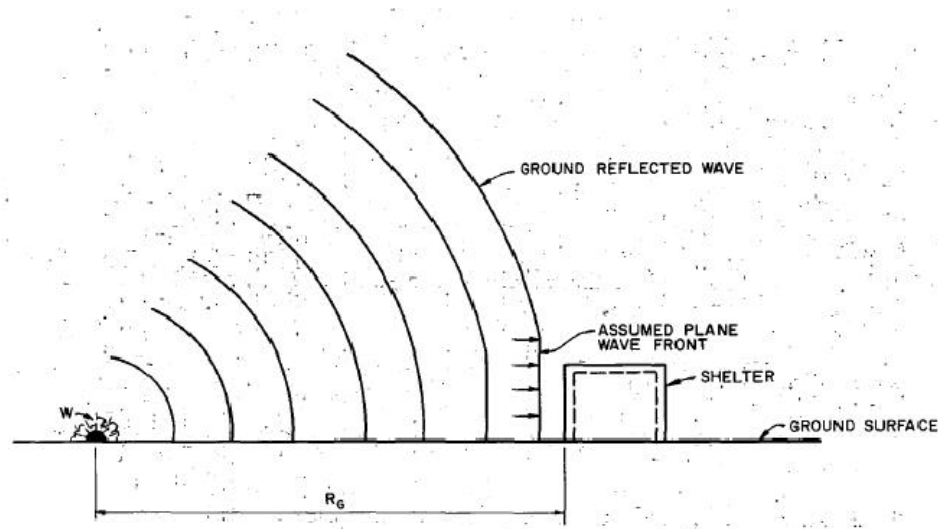


Figure 2-14 Surface burst blast environment

Figure 3-9: Hemispherical Blast Wave Diagram (Figure 2-14 TM5-1300) [19]

If the charge weight is large or the standoff distance is short, the magnitude can be much larger compared to the seismic load. This will be seen later in this section when charge weights and standoff distances are selected for testing. In considering a dynamic

analysis, the duration of the event differs between seismic and blast. An earthquake will last for a number of seconds where a pressure wave from a blast is over in a few microseconds. Therefore, the seismic load causes a longer loading phase than the blast case. Also, the earthquake acts throughout the depth of the structure. A blast will primarily act on the surface as the wave will dissipate as it gets deeper into the structure.

As mentioned before, a blast wave occurs in a few microseconds. During this time period, the structure experiences positive and negative pressure phases. A document developed by the Federal Emergency Management Association called “Reference Manual to Mitigate Potential Terrorist Attacks Against Buildings,” or FEMA 426, explains in depth the pressure phases [20]. Figure 3-10 shows Figure 4-1 from FEMA 426 which shows the positive and negative phases of a blast event. This figure also shows “Time of Arrival.” This time is the time it takes from the moment of the explosion to the pressure wave reaching the structure. Again this is dependent upon the charge weight and standoff distance. For testing purposes, the negative phase of the event is neglected due to its magnitude being much less than that of the positive phase.

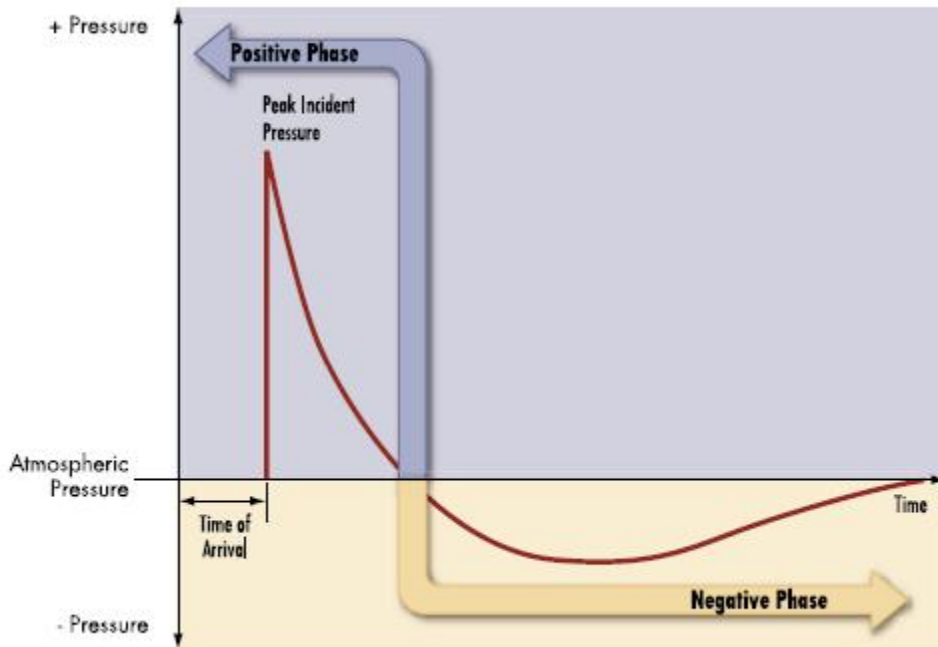
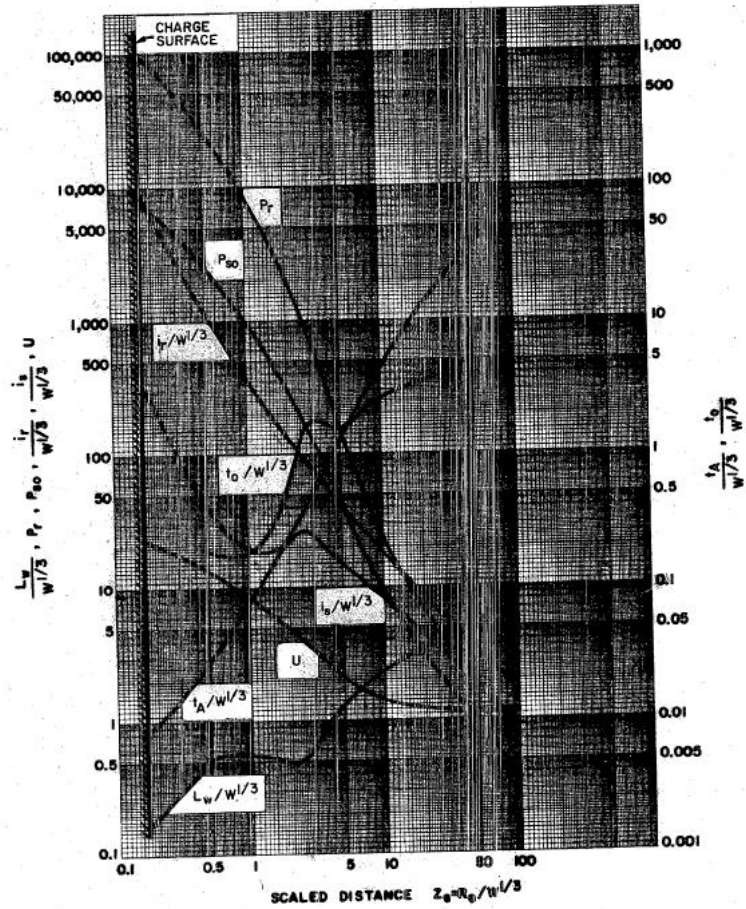


Figure 3-10: FEMA 426 Pressure-Time History [19]

To determine the magnitude of the positive peak pressure, TM5-1300 is used [19]. In this document, there are figures more commonly known as the “Spaghetti Charts.” These charts use scaled distance to determine peak pressure, impulse, arrival time, and duration of positive phase. These parameters are everything needed to develop not only the static blast pressure but also the time history function in order to complete a dynamic analysis. Figure 3-11 shows Figure 2-15 from the technical manual which is the figure used to determine the parameters for a hemispherical blast wave.



- $P_{s0}$  = PEAK POSITIVE INCIDENT PRESSURE, psi
- $P_r$  = PEAK POSITIVE NORMAL REFLECTED PRESSURE, psi
- $i_s/W^{1/3}$  = SCALED UNIT POSITIVE INCIDENT IMPULSE, psi-ms/lb<sup>1/3</sup>
- $i_r/W^{1/3}$  = SCALED UNIT POSITIVE NORMAL REFLECTED IMPULSE, psi-ms/lb<sup>1/3</sup>
- $t_0/W^{1/3}$  = SCALED TIME OF ARRIVAL OF BLAST WAVE, ms/lb<sup>1/3</sup>
- $t_A/W^{1/3}$  = SCALED POSITIVE DURATION OF POSITIVE PHASE, ms/lb<sup>1/3</sup>
- $U$  = SHOCK FRONT VELOCITY, ft/ms
- $W$  = CHARGE WEIGHT, lbs
- $L_w/W^{1/3}$  = SCALED WAVE LENGTH OF POSITIVE PHASE, ft/lb<sup>1/3</sup>

Figure 2-15 Positive phase shock wave parameters for a hemispherical TNT explosion on the surface at sea level

2-57

Figure 3-11: Hemispherical Blast Wave Parameters (Figure 2-15 TM5-1300) [19]

A hemispherical blast wave was chosen due to the likelihood that any threat to a building would be a surface burst, such as a truck, car, or hand carried explosive. Therefore, no airburst or spherical blast wave was used in this experiment.

With the background of blast loading understood, it is now possible to develop blast test cases for the steel frame model. First, charge weights and standoff distances needed to be chosen. FEMA 426 has a diagram showing possible charge sizes relative to the threat. It shows the possible size of a charge compared to different means of transport. It also shows minimum standoff distances for the effects listed in the figure. Figure 3-12 shows Figure 4-5 from FEMA 426 [20].

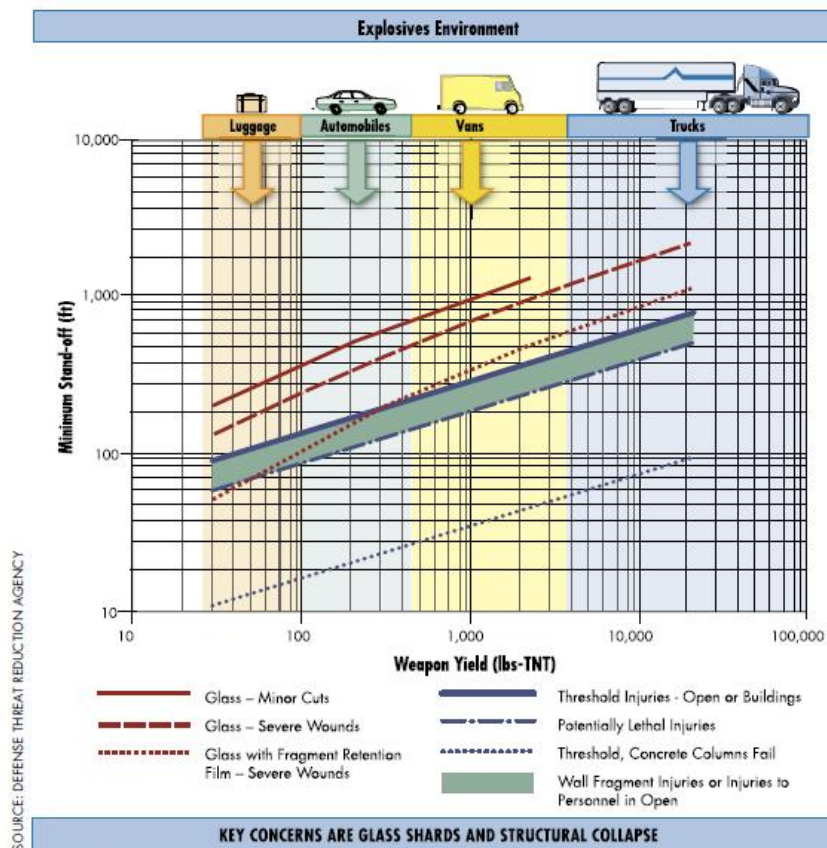


Figure 4-5 Explosives environments - blast range to effects

Figure 3-12: Possible Blast Charge Weights and Standoff (Figure 4-5 FEMA 426) [20]

Therefore using this plot, three charge weights and three standoff distances were chosen for a total of nine blast cases. Each charge weight was examined at each standoff distance. The charge weights were chosen for low, medium, and high yield explosions.

The standoff distances were also chosen in a similar method by using distances for close, medium, and far ranges. Once this parameter is chosen, the time history plots can be developed using the technical manual to determine parameters.

For the dynamic analysis and comparison to the dynamic earthquake loading, only one of the nine blast cases was used. The blast case chosen was that of median charge weight and standoff distance. The time history plot for this case is shown below in Figure 3-13 from SAP2000 after the time parameters were input. In this plot there is a calculated “Rise Time.” This rise time is used do to SAP2000’s inability to properly calculate the instantaneous loading of the blast wave. TM5-1300 also allows for the calculation of this rise time [19].

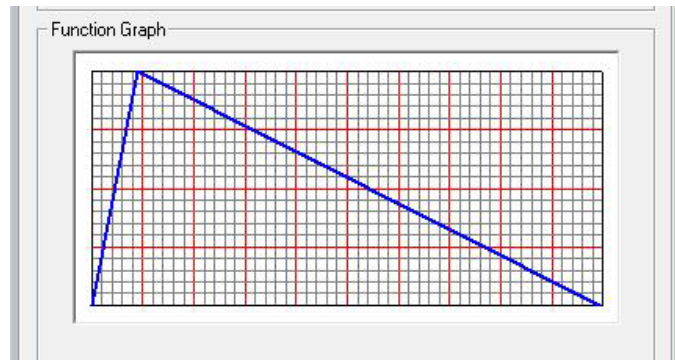


Figure 3-13: Time History Function for Blast Analysis

The dynamic load case results showed that indeed the blast case chosen was much larger than the 6.9 magnitude earthquake. The base reactions for the blast case were 96.16 Kips which are almost twice as high as the earthquake. Comparing the drift ratio also shows a significant difference. The calculated drift ratio for the blast is considered to be zero due to the actual value being  $3.611E-5$ . This also shows that due to the natural

period, the structure either does not have time to excite due to the blast, or the entire blast is absorbed by the structure.

The results from the static blast cases were used to determine the structures damage levels and survivability. In the next section, each of the nine cases are examined in depth to determine resistivity.

### 3.3 Frame Response to Blast Pressure

The static blast pressures were applied as line loads converted from pressure distributed over the wall area on the blast face. This allows for a distributed load on each column separately. To reference displacements and moments, the columns and joints were numbered from left to right and bottom to top of the blast face. Figures 3-14 and 3-15 show the column numbering and joint numbering, respectively.

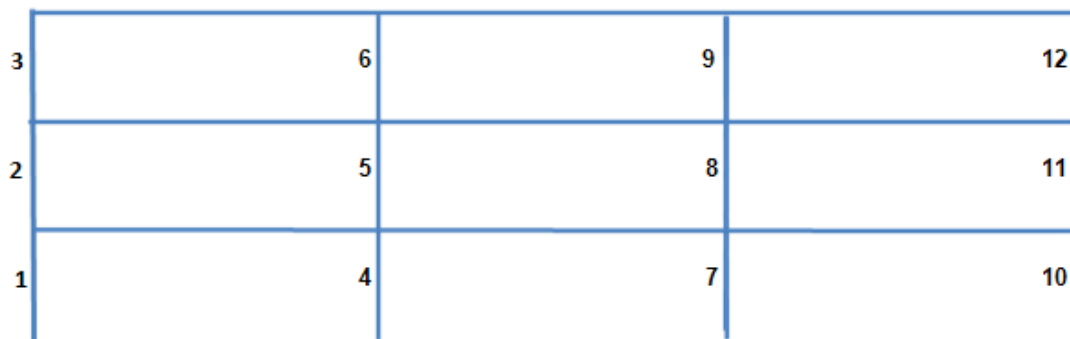


Figure 3-14: Column Numbering System to Monitor Blast Effects

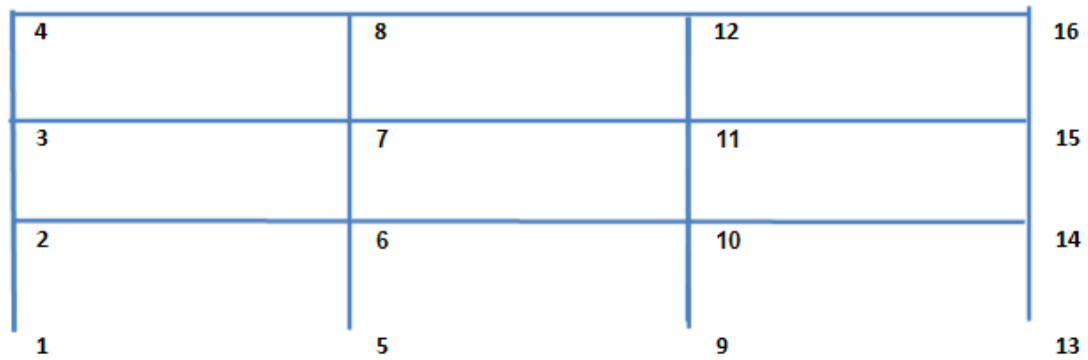


Figure 3-15: Joint Numbering System to Monitor Blast Effects

### 3.3.1 Close Standoff Distance

The first three test cases were at an extremely short standoff distance. This would fit a scenario where an individual were walking past the building or if a building were situated in a major city or downtown area near a road.

#### 3.3.1.1 Low Yield Charge Weight

The low yield charge does show that some yielding will occur due to the applied displacement values. The moment values show that a plastic hinge will not develop; therefore, there will not be any complete failures in the columns. There will be some yielding. Almost all of the columns have displacements greater than the value of first yield calculated in Chapter 2. It is also noted that each displacement is relatively the same. Table 3-1 shows the percent of plastic moment generated in each column and the drift at each joint.

Table 3-1: Percent of Plastic Moment and Drift from Low Yield Close Range

<b>Column Number</b>	<b><math>M_{max}/M_p</math> (%)</b>	<b>Joint</b>	<b>Drift</b>
<b>1</b>	9.56	<b>1</b>	0.000
<b>2</b>	0.99	<b>2</b>	0.010
<b>3</b>	0.21	<b>3</b>	0.010
<b>4</b>	3.51	<b>4</b>	0.010
<b>5</b>	0.74	<b>5</b>	0.010
<b>6</b>	0.55	<b>6</b>	0.011
<b>7</b>	4.73	<b>7</b>	0.011
<b>8</b>	0.53	<b>8</b>	0.011
<b>9</b>	0.53	<b>9</b>	0.000
<b>10</b>	9.51	<b>10</b>	0.010
<b>11</b>	0.96	<b>11</b>	0.010
<b>12</b>	0.21	<b>12</b>	0.010
		<b>13</b>	0.010
		<b>14</b>	0.010
		<b>15</b>	0.010
		<b>16</b>	0.010

From these displacements the drift index can be calculated. The drift index for this case is determined to be 0.01 which is still within code; therefore, the structure is still considered suitable for immediate occupancy according to FEMA 356 which is used to assess buildings after seismic events [21]. It can be concluded that this low yield blast will have little effect on the survivability of this structure.

### 3.3.1.2 Medium Yield Charge Weight

The medium yield charge is similar to the low yield in that there are no plastic hinge formations and therefore there are no complete failures. However, the displacement is large enough to fall beyond the range of the calculated elastic buckling displacement. This is a major cause for concern because the structure may be subject to collapse if it has not already done so. The elastic buckling calculations mentioned in

Chapter 2 were calculated using a more extreme case than this. Therefore it can be assumed that the structure will not have buckled but may buckle with any major reloading. Table 3-2 shows the percent of plastic moment and drift caused by the medium yield blast.

Table 3-2: Percent of Plastic Moment and Drift from Medium Yield Close Range

<b>Column Number</b>	<b><math>M_{max}/M_p</math> (%)</b>	<b>Joint</b>	<b>Drift</b>
<b>1</b>	21.19	<b>1</b>	0.000
<b>2</b>	2.94	<b>2</b>	0.021
<b>3</b>	0.67	<b>3</b>	0.021
<b>4</b>	8.79	<b>4</b>	0.024
<b>5</b>	2.40	<b>5</b>	0.024
<b>6</b>	1.46	<b>6</b>	0.024
<b>7</b>	12.15	<b>7</b>	0.024
<b>8</b>	1.38	<b>8</b>	0.024
<b>9</b>	1.38	<b>9</b>	0.000
<b>10</b>	21.04	<b>10</b>	0.021
<b>11</b>	2.84	<b>11</b>	0.021
<b>12</b>	0.67	<b>12</b>	0.023
		<b>13</b>	0.023
		<b>14</b>	0.024
		<b>15</b>	0.024
		<b>16</b>	0.024

The drift index of this case does exceed FEMA 356 standard at 0.023 which indicates there will be potential life safety hazards [21]. Thus, it would not be cleared for immediate occupancy.

### 3.3.1.3 High Yield Charge Weight

The high yield case at close distance shows considerable damage. Two of the lower level columns have developed a plastic hinge and are deemed unable to carry any further load. Columns 4 and 7 both have reached a plastic hinge. These two columns are

closest to the blast. Columns 1 and 10 also have significant damage being that their moments are close to 40 percent of that of the plastic hinge development. The displacements in all locations exceed that of any of the calculations previously completed thus major damage has occurred. Table 3-3 shows the percent of plastic moment and drift for this case.

Table 3-3: Percent of Plastic Moment and Drift for High Yield Close Range

<b>Column Number</b>	<b><math>M_{max}/M_p</math> (%)</b>	<b>Joint</b>	<b>Drift</b>
<b>1</b>	36.46	<b>1</b>	0.000
<b>2</b>	10.22	<b>2</b>	0.129
<b>3</b>	1.78	<b>3</b>	0.129
<b>4</b>	100.81	<b>4</b>	0.137
<b>5</b>	-7.22	<b>5</b>	0.137
<b>6</b>	5.16	<b>6</b>	0.138
<b>7</b>	125.90	<b>7</b>	0.138
<b>8</b>	4.48	<b>8</b>	0.138
<b>9</b>	4.48	<b>9</b>	0.000
<b>10</b>	39.88	<b>10</b>	0.126
<b>11</b>	8.98	<b>11</b>	0.126
<b>12</b>	1.82	<b>12</b>	0.134
		<b>13</b>	0.134
		<b>14</b>	0.135
		<b>15</b>	0.135
		<b>16</b>	0.135

With this obvious amount of damage, the drift ratio is exceeded tremendously as it is equal to 0.135 which is well above the safe 0.02. This building would collapse and there would be catastrophic damage.

### 3.3.2 Medium Standoff Distance

The medium standoff distance shows less damage than the close range. This scenario would present itself in less dense areas and areas where access to the building

can be monitored, but the entire complex, to include parking, does not have controlled access.

### 3.3.2.1 Low Yield Charge Weight

This case shows that there could possibly be minor yielding in some of the columns but nothing major to cause any alarm. The maximum displacements recorded show that the only criteria exceeded would be the first yield of the fixed-fixed and simply supported in the linear elastic case. The moments generated are not anywhere near a yield point. Table 3-4 shows the results.

Table 3-4: Percent of Plastic Moment and Drift for Low Yield Medium Range

<b>Column Number</b>	<b><math>M_{max}/M_p</math> (%)</b>	<b>Joint</b>	<b>Drift</b>
<b>1</b>	5.06	<b>1</b>	0.000
<b>2</b>	1.21	<b>2</b>	0.005
<b>3</b>	0.48	<b>3</b>	0.005
<b>4</b>	3.29	<b>4</b>	0.006
<b>5</b>	0.46	<b>5</b>	0.006
<b>6</b>	0.75	<b>6</b>	0.006
<b>7</b>	4.42	<b>7</b>	0.006
<b>8</b>	0.72	<b>8</b>	0.006
<b>9</b>	0.72	<b>9</b>	0.000
<b>10</b>	5.00	<b>10</b>	0.005
<b>11</b>	1.18	<b>11</b>	0.005
<b>12</b>	0.48	<b>12</b>	0.006
		<b>13</b>	0.006
		<b>14</b>	0.006
		<b>15</b>	0.006
		<b>16</b>	0.006

For comparison purposes, the drift ratio for this case is 0.006 which is well below the 0.02 requirement. Immediate occupancy would be authorized.

### 3.3.2.2 Medium Yield Charge Weight

There is very little difference between the medium and low yield cases at this distance. As in the low yield case, the only displacement parameters exceeded are that of the first yield calculations. The moments generated are larger than that of the low yield but again do not exceed any critical states. Table 3-5 shows the percent of plastic moment and drift.

Table 3-5: Percent of Plastic Moment and Drift for Medium Yield Medium Range

<b>Column Number</b>	<b><math>M_{max}/M_p</math> (%)</b>	<b>Joint</b>	<b>Drift</b>
<b>1</b>	6.91	<b>1</b>	0.000
<b>2</b>	1.54	<b>2</b>	0.007
<b>3</b>	0.67	<b>3</b>	0.007
<b>4</b>	4.25	<b>4</b>	0.008
<b>5</b>	0.59	<b>5</b>	0.008
<b>6</b>	0.97	<b>6</b>	0.009
<b>7</b>	5.71	<b>7</b>	0.009
<b>8</b>	0.93	<b>8</b>	0.009
<b>9</b>	0.93	<b>9</b>	0.000
<b>10</b>	6.83	<b>10</b>	0.007
<b>11</b>	1.50	<b>11</b>	0.007
<b>12</b>	0.67	<b>12</b>	0.008
		<b>13</b>	0.008
		<b>14</b>	0.009
		<b>15</b>	0.009
		<b>16</b>	0.009

The drift ratio parameter is not exceeded in this case either with this case having a drift ratio of 0.008 and allows for immediate occupancy.

### 3.3.2.3 High Yield Charge Weight

This scenario does not show any difference between the previous two as well. The values are slightly larger but not large enough to meet any other damage criteria.

The displacements show some yielding, and the moments do not reach any critical value.

Table 3-6 summarizes the results.

Table 3-6: Percent of Plastic Moment and Drift for High Yield Medium Range

<b>Column Number</b>	<b><math>M_{max}/M_p</math> (%)</b>	<b>Joint</b>	<b>Drift</b>
<b>1</b>	5.78	<b>1</b>	0.000
<b>2</b>	2.13	<b>2</b>	0.006
<b>3</b>	0.86	<b>3</b>	0.006
<b>4</b>	5.30	<b>4</b>	0.008
<b>5</b>	0.76	<b>5</b>	0.008
<b>6</b>	1.36	<b>6</b>	0.008
<b>7</b>	7.19	<b>7</b>	0.008
<b>8</b>	1.32	<b>8</b>	0.008
<b>9</b>	1.32	<b>9</b>	0.000
<b>10</b>	5.67	<b>10</b>	0.006
<b>11</b>	2.08	<b>11</b>	0.006
<b>12</b>	0.86	<b>12</b>	0.008
		<b>13</b>	0.008
		<b>14</b>	0.008
		<b>15</b>	0.008
		<b>16</b>	0.008

The drift ratio for this case is also insignificant, 0.007, and allows for immediate occupancy.

### 3.3.3 Far Standoff Distance

As shown in the previous section, the charge weights shown have no significant effect on the structure at the medium range. Therefore, there will be no change for the farther distance. This distant of a scenario would develop from a location that could possibly have controlled access not only to the building but the surrounding parking areas as well. The percent of plastic moment and drift values are shown in Table 3-7 and 3-8

for all three charge yield cases. For all cases the drift ratio is safe for immediate occupancy.

Table 3-7: Percent of Plastic Moment for Low, Medium, and High Yield Far Range

<b>Column Number</b>	<b>Low Yield</b>	<b>Medium Yield</b> $M_{max}/M_p$ (%)	<b>High Yield</b>
<b>1</b>	0.321	0.823	1.859
<b>2</b>	0.061	0.335	0.749
<b>3</b>	0.028	0.139	0.312
<b>4</b>	0.175	0.795	1.782
<b>5</b>	0.024	0.113	0.253
<b>6</b>	0.040	0.201	0.450
<b>7</b>	0.234	1.078	2.416
<b>8</b>	0.039	0.194	0.436
<b>9</b>	0.039	0.194	0.436
<b>10</b>	0.318	0.806	1.822
<b>11</b>	0.060	0.326	0.731
<b>12</b>	0.028	0.140	0.313

Table 3-8: Drift for Low, Medium, and High Yield Far Range

<b>Joint</b>	<b>Low Yield</b>	<b>Medium Yield</b> <b>Drift</b>	<b>High Yield</b>
<b>1</b>	0.00000	0.000	0.000
<b>2</b>	0.00033	0.001	0.002
<b>3</b>	0.00038	0.001	0.002
<b>4</b>	0.00039	0.001	0.003
<b>5</b>	0.00000	0.000	0.000
<b>6</b>	0.00033	0.001	0.002
<b>7</b>	0.00037	0.001	0.002
<b>8</b>	0.00039	0.001	0.003
<b>9</b>	0.00000	0.000	0.000
<b>10</b>	0.00033	0.001	0.002
<b>11</b>	0.00037	0.001	0.002
<b>12</b>	0.00039	0.001	0.003
<b>13</b>	0.00000	0.000	0.000
<b>14</b>	0.00033	0.001	0.002
<b>15</b>	0.00037	0.001	0.002
<b>16</b>	0.00038	0.001	0.003



## CHAPTER IV

### CONCLUSIONS AND RECOMMENDATIONS

#### 4.1 Conclusions

The results of these models show major performance differences. The only model case to produce reasonable results was the fixed-fixed rotation case. In this case, the Moment-Rotation curve was able to be taken to the plastic limit therefore demonstrating that the plastic hinge has developed. Referencing this curve to the Force-Displacement curve allows for the determination of a load, or pressure, at which not only the plastic hinge develops but also at different damage levels throughout the life of the column.

The other two model cases, fixed-free rotation and pinned-free rotation, are going to require further investigation. These two models would not allow the displacement to reach its input limit without convergence issues. After reducing the limitations on both, better defined curves were generated; however, these results did not show that any significant limit states had been reached. A fully plastic moment was never achieved in either model though the reaction force developed a plateau or began to degrade. The only explanation for these results is that the step size generated by SAP2000 was too large to properly monitor the performance throughout the life cycle of the column. This also prevents a more detailed investigation to determine if there are any other failure criteria being met.

Overall, the data that was able to be extracted was used to complete the investigation of the three dimensional frame which was checked by analytical

calculations in order to more accurately determine limit states and to prove the models validity. These limits provided the damage criteria for the columns in the frame model. This allowed the column response in the frame model to be compared to the damage levels developed in the individual column. First yield, elastic buckling, and plastic hinge formation were all used as break point in the damage levels of the columns on the blast face of the three-dimensional frame.

As for the three-dimensional frame, the blast cases chosen turned out to be relatively weak for steel structures. Only the high yield at close range showed any mechanism of failure. There were some minor yielding occurring in most of the other cases, but nothing was significant enough to raise any major alarms. This confirms as many have said that the best way to mitigate blast damage is to increase the standoff distance. Many buildings of high importance have implemented protection plans and devices to force the standoff distance to be increased.

Furthermore, buildings designed for multiple hazards do show an increased resistivity to numerous hazards to include blast. The similarities between seismic and blast loading allow for seismically designed structures to have a natural higher resistance to blast than those without seismic design. However due to the wide range of blast loading, a seismically designed structure is not guaranteed to have a resistance to blast. It is recommended not only to design for multi-hazards but also to design specifically for a blast scenario if the structure has the possible threat. This will increase the survivability of not only the structure but the occupants as well.

## 4.2 Recommendations for Future Work

For future investigation into column analysis, it is recommended that different software be used. A general purpose non-linear finite element software is suggested with the availability to modify step size is critical, and the ability to more closely monitor the flange and web performance should be used.

There are numerous recommendations to improve the study of the frame system and further advance the knowledge of multi-hazard structures and blast resistance.

1. Further investigation into blast resistivity of steel structures is needed. The nine cases chosen in this experiment do not demonstrate a reasonable range of resistivity. Numerous section sizes and building heights need to be explored.
2. Charge weights need to be increased. It may be possible to increase the database by using only one standoff distance or one charge weight. This would allow for only one changing parameter would which would give a better range of damage and resistivity.
3. A more in-depth computer model is also encouraged. The boundary conditions in the three dimensional frame are not exactly as the column analysis depicts. The use of a spring system may be the solution.
4. Dynamic analysis is also encouraged due to a more accurate assessment of damage.

## LIST OF REFERENCES

## LIST OF REFERENCES

1. Sabuwala, T., D. Linzell, and T. Krauthammer, *Finite element analysis of steel beam to column connections subjected to blast loads*. International Journal of Impact Engineering, 2005. **31**(7): p. 861-876.
2. Karns, J.E., et al., *Analytical Verification of Blast Testing of Steel Frame Moment Connection Assemblies, Structures Congress 2007*. 2007, ASCE. p. 19.
3. Lee, K., *Local response of W-shaped steel columns under blast loading*. Structural Engineering and Mechanics, 2009. **31**(1): p. 25-38.
4. Montalva, A., J. Godinho, and S. Marjanishvili, *Air-Blast Failure Criteria for Columns Using Finite Element Methods, Structures Congress 2008*. 2008, ASCE. p. 10.
5. Hwang, Y.S. and J.C. Anderson, *Response of a Low Rise Steel Building to Air Blast*, in *Structures Congress 2008*. 2008, ASCE. p. 12.
6. American Institute of Steel Construction, Inc., *Steel Construction Manual*. 13 ed. 2005.
7. Tadepalli, T., *Performance Evaluation of Low-Rise Concrete Frame Building Structures in Moderate Seismic Zones Subject to External Blast Loading*, in *Department of Civil Engineering*. 2009, University of Mississippi: Oxford, MS.
8. Computers and Structures, Inc., *SAP2000 Version 12 User's Manual*. 2008, Berkeley, CA.
9. Galambos, T.V. and A.E. Surovek, *Structural Stability of Steel: Concepts and Applications for Structural Engineers*. 2008, Hoboken, New Jersey: John Wiley & Sons, Inc. 373.
10. Neal, B.G., *The Plastic Methods of Structural Analysis*. 3rd ed. 1977, London: Chapman and Hall Ltd. 200.
11. Gere, J.M., *Mechanics of Materials*. 6th ed. 2004, Belmont, CA: Brooks/Cole-Thomson Learning. 940.
12. International Code Council, Inc., *2006 International Building Code*. 2006.
13. American Society of Civil Engineers., *ASCE 7-05: Minimum Design Loads for Buildings and Other Structures*. 2005.

14. American Concrete Institute., *ACI 310-05: Standard Specifications for Structural Concrete*. 2005.
15. McCormac, J.C., *Structural Steel Design*. 4th ed. 2008, Upper Saddle River, NJ: Pearson Prentice Hall.
16. Salmon, C.G., J.E. Johnson, and F.A. Malhas, *Steel Structures Design and Behavior*. 5th ed. 2009, Upper Saddle River, NJ: Pearson Prentice Hall.
17. Structures and Codes Institute., *CodeMaster: Seismic Design*, S.K.G.A. Inc., Editor. 2007.
18. United States Geological Survey. *Hazards*. 2009. cited 2009; Available from: <http://earthquake.usgs.gov/research/hazmaps>.
19. *TM5-1300: Structures to Resist the Effects of Accidental Explosions*, Departments of the Army, and the Air Force, Editor. 1990: Washington, DC.
20. Federal Emergency Management Agency, *FEMA 426: Reference Manual to Mitigate Potential Terrorist Attacks Against Buildings*.
21. Federal Emergency Management Agency, *FEMA 356: Prestandard and Commentary for the Seismic Rehabilitation of Buildings*. 2000.

## LIST OF APPENDICIES

# APPENDIX A

## FIXED-FREE ROTATION RESULTS

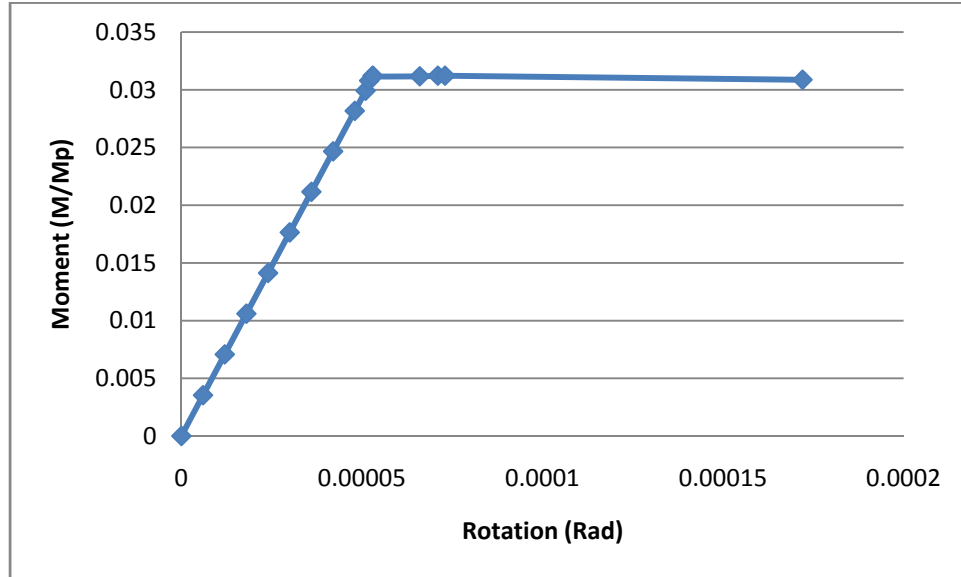


Figure A-1: Moment-Rotation Curve for Fixed-Free Rotation

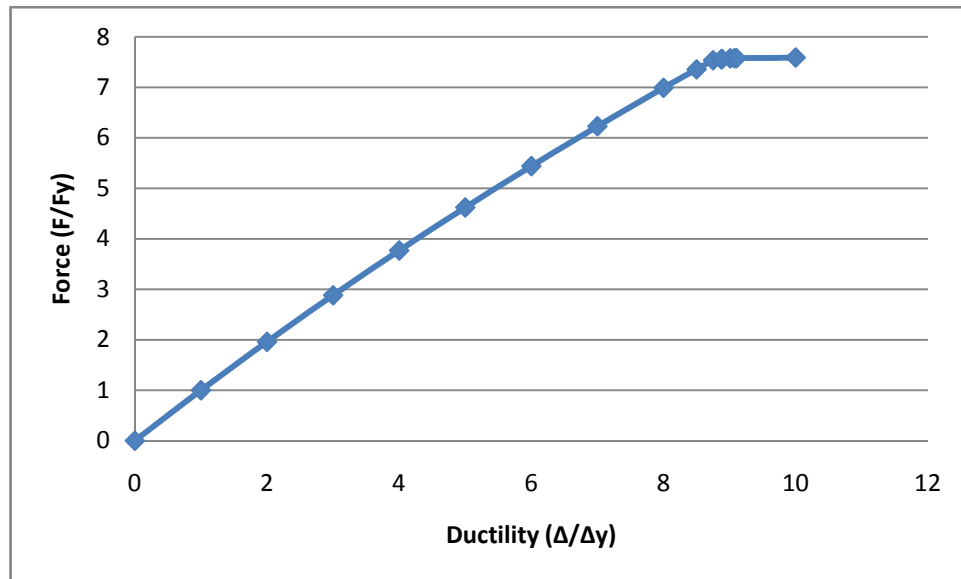


Figure A-2: Force-Ductility for Fixed-Free Rotation

## APPENDIX B

### PINNED-FREE ROTATION RESULTS

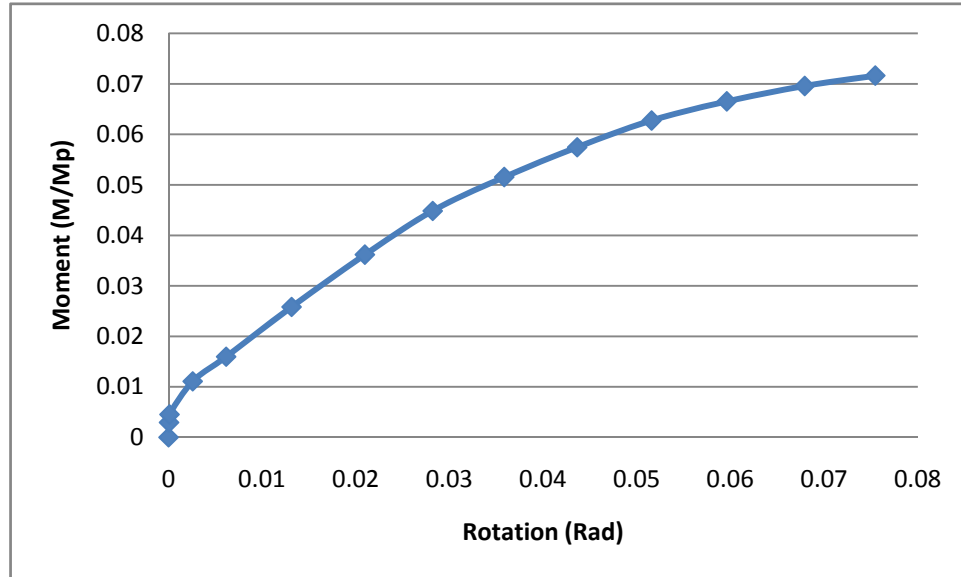


Figure B-1: Moment-Rotation Curve for Pinned-Free Rotation

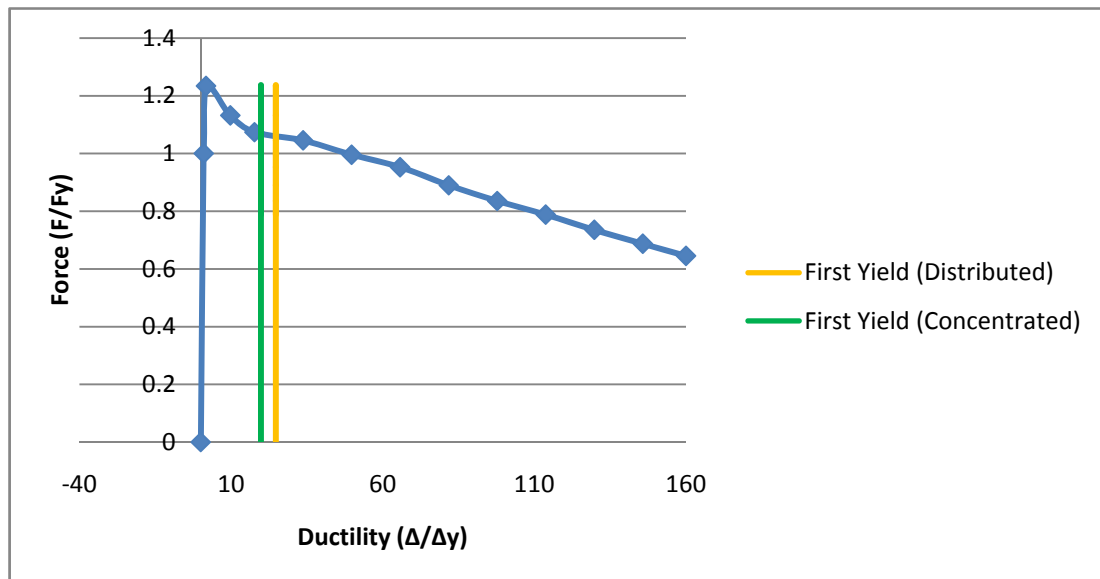


Figure B-2: Force-Ductility Curve for Pinned-Free Rotation